THESIS

STRUCTURAL ANALYSIS ALONG THE OURAY FAULT, SOUTHWESTERN COLORADO: IMPLICATIONS FOR THE KINEMATIC DEVELOPMENT OF THE LATE PALEOZOIC ANCESTRAL ROCKY MOUNTAINS

Submitted by

Erinn P. Johnson

Department of Geosciences

In partial fulfillment of the requirements

For the Degree of Master of Science

Colorado State University

Fort Collins, Colorado

Fall 2021

Master's Committee:

Advisor: John Singleton

Sally Sutton
Julia Sharp

ABSTRACT

STRUCTURAL ANALYSIS ALONG THE OURAY FAULT, SOUTHWESTERN COLORADO: IMPLICATIONS FOR THE KINEMATIC DEVELOPMENT OF THE LATE PALEOZOIC ANCESTRAL ROCKY MOUNTAINS

The Ouray fault in southwest Colorado provides insight into the geometry and kinematics of deformation during the formation of the late Paleozoic Ancestral Rocky Mountains (ARM). The Ouray fault strikes WNW-ESE and dips subvertically to steeply south, juxtaposing the Paleoproterozoic Uncompahgre Group on the south side against Mississippian-Pennsylvanian strata on the north side. Kinematic data from the Ouray fault, adjacent small-scale faults, the observed offset, and folds in Paleozoic strata indicate that the Ouray fault records sinistral transpression. Using the average 15° W-plunging slickenlines from the principal slip plane, we estimate the total oblique sinistral displacement of the fault to be ~600 to 800 m. The uniformly overlapping Mesozoic strata atop the projected trace of the Ouray fault indicate that the fault is a preserved ARM structure not reactivated during the Laramide orogeny. The Ouray fault is oriented subparallel to the Uncompahgre Group bedding and follows the weaker Uncompahgre phyllite for most of its length, suggesting the preexisting structures within the Uncompahgre Group greatly influenced the orientation of the Ouray fault. N-S- to NW-SE-striking joints and quartz veins in all geologic units spanning the Paleoproterozoic to the Cenozoic postdate slip on the Ouray fault and likely formed during Cenozoic magmatism. A sample of calcite from the principal slip plane of the Ouray fault yielded a U-Pb date of 39.3 ± 6.2 Ma. I interpret this date to record resetting by late Eocene hydrothermal fluid flow. The record of strain around the Ouray fault may be representative of the southwestern margin of the Ancestral Uncompahgre uplift in Colorado. This study supports recent tectonic models for the ARM system which propose that ARM uplift was driven by NE-SW compression during the Pennsylvanian and Permian periods.

ACKNOWLEDGEMENTS

I would like to start out by thanking landowners Dave C. and Sandor R. for allowing us access to their properties, which were essential areas for this project. A big thanks to Deere and Ault Consultants for their support and flexibility while I completed this endeavor. Thank you to my family and friends for their help and support throughout this process. A special thank you to Jabe and Eve for welcoming me into their home for most my time as a master's student. I will be eternally grateful for your kindness and support during that time. Thank you to Jake and Maui, for being my field assistants and overall support. Thank you to my committee members Dr. Sally Sutton and Dr. Julia Sharp. Last but not least, thank you to Dr. John Singleton for taking me on as a student when my other project fell through, and for all his help along the way.

//

I acknowledge the Southern Ute and Pueblo peoples; the traditional stewards of the Ouray region, and I pay my respects to their elders past and present.

Colorado State University acknowledges, with respect, that the land we are on today is the traditional and ancestral homelands of the Arapaho, Cheyenne, and Ute Nations and peoples. This was also a site of trade, gathering, and healing for numerous other Native tribes. We recognize the Indigenous peoples as original stewards of this land and all the relatives within it. As these words of acknowledgment are spoken and heard, the ties Nations have to their traditional homelands are renewed and reaffirmed.

CSU is founded as a land-grant institution, and we accept that our mission must encompass access to education and inclusion. And, significantly, that our founding came at a dire cost to Native Nations and peoples whose land this University was built upon. This acknowledgment is the education and inclusion we must practice in recognizing our institutional history, responsibility, and commitment.

TABLE OF CONTENTS

LIST OF FIGURES

LIST OF SUPPLEMENTARY MATERIALS

1.0 INTRODUCTION

1.1 Ancestral Rocky Mountain System

The Ancestral Rocky Mountains (ARM) formed during a cryptic orogenic event in the late Paleozoic. The ARM system consists of Early Pennsylvanian to early Permian uplifts and juxtaposed hydrocarbon-rich basins. Most of what we know about the ARM comes from the sedimentary record, and from oil field drilling and other subsurface data collected in these basins (e.g., Stone, 1977; Shumaker, 1992; Frahme and Vaughn, 1983; McConnell, 1989; Ye et al., 1996; Turko and Mitra, 2021). Relatively little is known about the geometry and kinematics of structures leading to the ARM uplift. Many of the structures from this orogenic event have limited exposures in the rock record, and many were overprinted by the subsequent Late Cretaceous - early Paleogene Laramide orogeny. Examples of Laramide deformation overprinting ARM structures include the Ute Pass reverse fault near Colorado Springs, Colorado (Kluth, 1997; Sweet and Soreghan, 2010) and the Gore fault near Vail, Colorado (Tweto and Lovering, 1977; Kluth, 1997). There is a wealth of kinematic data on Laramide deformation (e.g., Erslev, 2001; Caine et al., 2006; Erslev and Koenig, 2009; Weil and Yonkee, 2012; Singleton et al., 2019); however, comparable studies for the ARM kinematics are rare to nonexistent.

The ARM system is considered to be a predominantly NW-SE oriented, intraplate, basement-involved uplift and basin-forming event stretching across Utah, Colorado, Oklahoma, New Mexico and Texas (Figure 1) (Kluth and Coney, 1981; Ye et al., 1996; Hoy and Ridgway, 2002; Barbeau, 2003; Soreghan et al., 2012; Leary et al., 2017, 2020; Sweet et al., 2021). The ARM uplifts are typically interpreted to be bound by NW-SE striking reverse faults, whose movement likely resulted in the flexural basins surrounding the uplifts (Ye et al., 1996; Barbeau, 2003; Hoy and Ridgway, 2002; Sweet and Soreghan, 2010; Leary et al., 2020; Sweet et al., 2021). The major uplifts in the system are the Uncompahgre, Ancestral Front Range, and Wichita uplifts, with approximately seven minor uplifts. Major basins of the ARM system include the Paradox, Eagle-Central Colorado Trough, Denver, Anadarko, Palo Duro, and Orogrande basins (Figure 1).

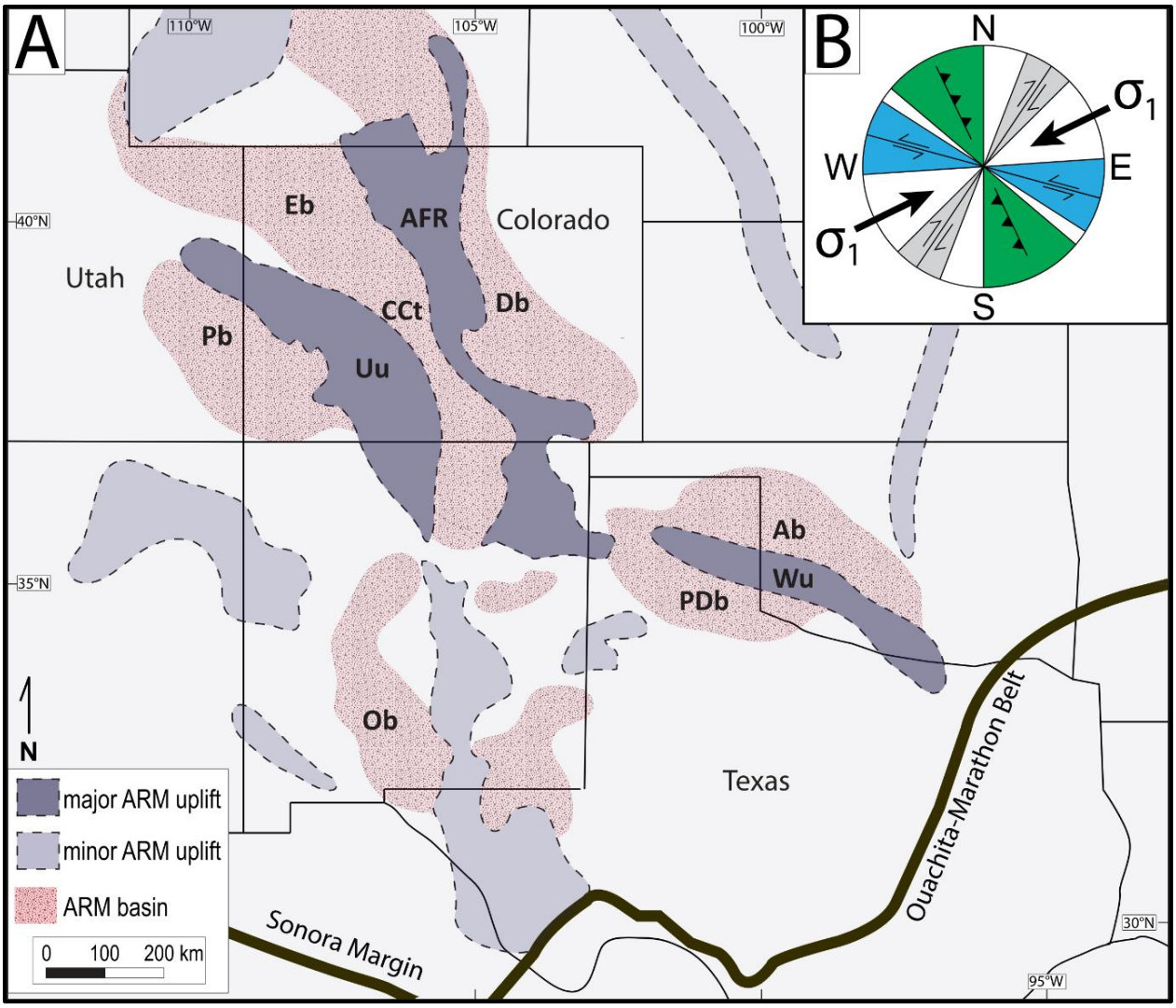

Figure 1. A) Simplified map showing the locations of major and minor Ancestral Rocky Mountain (ARM) uplifts and associated sedimentary basins (locations modified from Soreghan et al. (2012) and Sweet et al. (2015)). Major ARM system features mentioned in the text: Uu = Uncompahgre uplift; AFR = Ancestral Front Range; Wu = Wichita uplift; Eb = Eagle basin; CCt = Central Colorado trough; Pb = Paradox basin; Db = Denver basin; Ab = Anadarko basin; PDb = Palo Duro basin; Ob = Orogrande. B) Kinematic model from Leary et al. (2017) from data collected in the Central Basin Platform (Shumaker, 1992) to predict orientations of ARM faults that may have formed in response to a regional NE-SW directed maximum stress.

Several major tectonic events occurred during the main phase of the Pennsylvanian ARM uplift, and many models attribute these events to ARM formation. This tectonism includes the NW-directed convergence across the Ouachita-Marathon collision belt (Kluth and Coney, 1981; Kluth, 1986; Dickinson and Lawton, 2003), left-lateral shear along transcontinental faults (Budnik, 1986), potential NE-directed flat-slab subduction along the Sonoran margin (Ye et al., 1996), reactivation of pre-existing rift features (Marshak et al., 2000; Soreghan et al., 2012), and oblique convergence along the Sonora margin (Leary

et al., 2017; Lawton et al., 2017; Sweet et al., 2021) (Figure 1). Regardless of the tectonic drivers of ARM formation, several studies have confirmed that ARM structures are compatible with NE-SW directed-intraplate shortening during the Pennsylvanian and Permian (Shumaker, 1992; Ye et al., 1996; Hoy and Ridgway, 2002; Thomas, 2007; Sweet and Soreghan, 2010; Leary et al., 2017; Sweet et al., 2021).

The classic model of ARM formation and tectonism stems from the Ouachita-Marathon orogeny as the primary driving force. The Ouachita-Marathon orogeny was the result of continental plate suturing in the southeastern United States (Kluth and Coney, 1981; Kluth, 1986; Dickinson and Lawton, 2003). In this model the ARM system is the result of foreland deformation from the Ouachita-Marathon orogeny. This model, however, does not account for NE-SW shortening recorded by ARM structures. Ye et al. (1996) proposed that the ARM system was more likely a result of NE-directed flat-slab subduction and intraplate shortening at the southwestern Sonora margin. However, there is no evidence of arc magmatism during the main phase of the Pennsylvanian ARM uplift.

Leary et al. (2017) proposed that the oblique convergence along the Sonora margin coupled with convergence across the Ouachita-Marathon margin and possibly the Nevada margin drove ARM formation. The Sonora margin records sinistral transpression during this time, possibly setting up the stress field responsible for NE-SW shortening across the ARM system (Leary et al., 2017; Lawton et al., 2017) (Figure 1b).

While several studies address tectonic drivers of the ARM system (e.g., Kluth and Coney, 1981; Budnik, 1986; Ye et al., 1996; Marshak et al., 2000; Dickinson and Lawton, 2003; Soreghan et al., 2012, Leary et al., 2017; Lawton et al., 2017; Lawton et al., 2020; Sweet et al., 2021) there is little geometric and kinematic data on ARM structures, which would benefit future models. A major goal of this study is to add kinematic and geometric data of ARM deformation by analyzing the Ouray fault along the southwestern margin of the Uncompahgre uplift.

1.2 Uncompahgre Uplift and Regional Geology

The Uncompahgre uplift and the adjacent Paradox basin are among the largest features of the ARM system stretching from eastern Utah, southwestern Colorado into northern New Mexico for approximately 500 km (Figure 1). The Uncompahgre uplift is bound to the SW by the Paradox basin and

to the NE by the Eagle basin and Central Colorado trough (CCT) (Figure 1, Figure 2). These basins are thought to have formed as flexural basins during contractional orogenesis and accumulated several kilometers of Pennsylvanian and Permian strata (Hoy and Ridgway, 2002; Barbeau, 2003). The Eagle basin and the Paradox basin, especially, have been exploited for their hydrocarbon resources. The Uncompahgre uplift has also been exploited for its mineral resources resulting from Laramide and late Eocene to early Miocene magmatism, with peak volcanism ~35–30 Ma (Steven and Lipman, 1976).

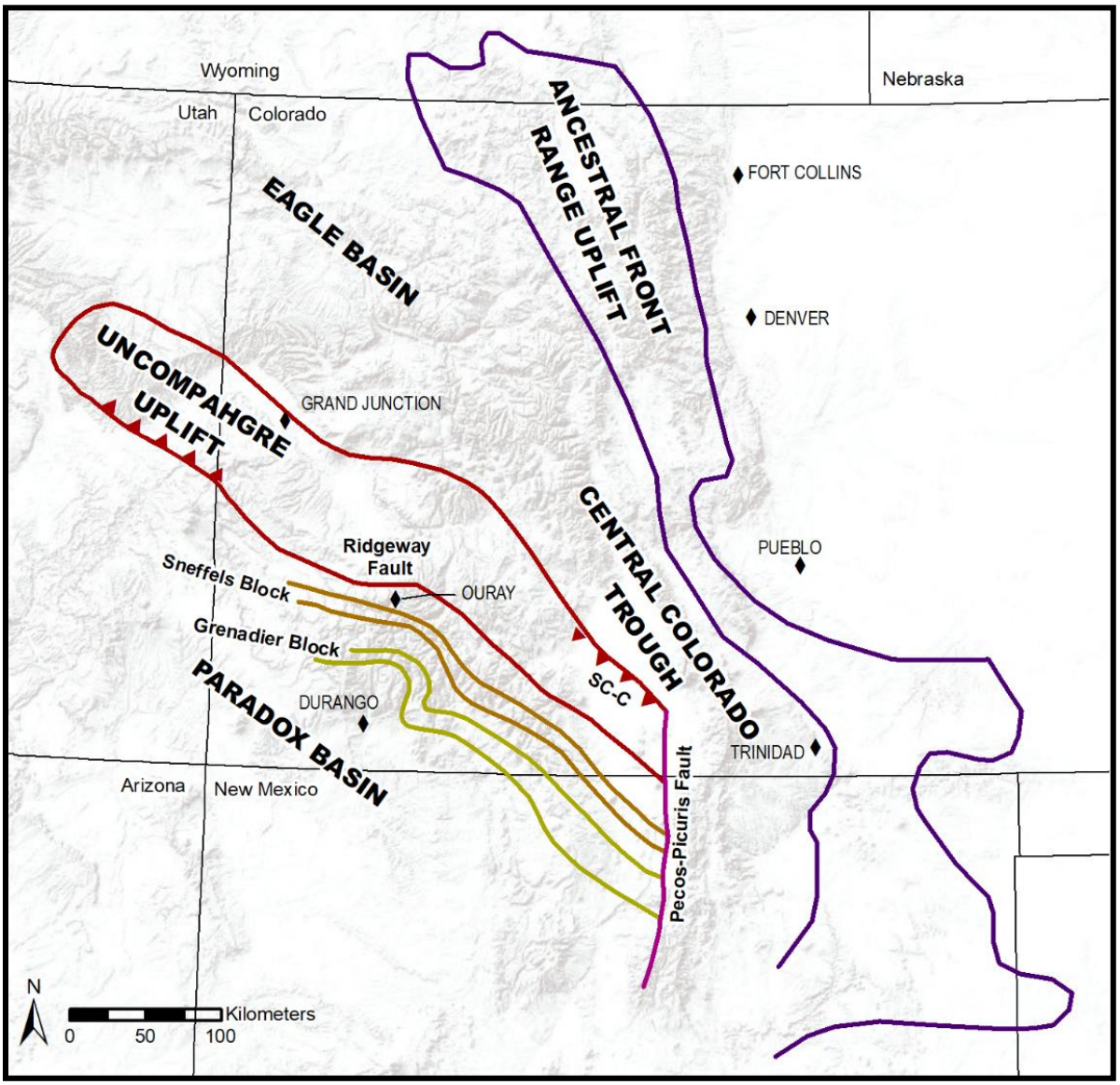

Figure 2. Index map of Ancestral Rocky Mountains, showing locations of faults along the boundary between the Uncompahgre uplift and the Paradox basin. After Thomas (2007) who compiled the map from Larsen and Cross (1956); Baars and See (1968); Weimer (1980); Frahme and Vaughn (1983); Hoy and Ridgway (2002). SC-C – Sand Creek-Crestone fault.

This prominent ARM feature has numerous interpretations for the faulting along its margins. The northeastern margin of the Uncompahgre uplift is defined by a system of SW-dipping thrust faults exposed in the Sangre de Cristo Mountains (Figure 2), with the synorogenic sedimentation focused within the adjacent CCT (Hoy and Ridgway, 2002). Hoy and Ridgway (2002) determined from geologic mapping of Pennsylvanian-Permian strata in the CCT that there was NE-SW shortening during the formation of the basin. Based on seismic data, De Voto et al. (1986) and Wachter and Johnson (1986) interpret the northeastern side of the Uncompahgre uplift to be bound by high-angle faults with unknown kinematics (Kluth, 1998).

Numerous tectonic/structural models exist for the southwestern margin of the Uncompahgre uplift. Based on seismic data and drill holes, several investigations have interpreted the margin between the Uncompahgre uplift and the Paradox basin as a moderately NE-dipping reverse fault which may have accommodated approximately 10 km of shortening (Stone, 1977; Frahme and Vaughn, 1983; Barbeau, 2003; Moore et al., 2008). Alternatively, the southwestern margin of the Uncompahgre uplift may record a significant component of sinistral slip, particularly along more E-W oriented portions of the uplift (Budnick, 1986; Thomas, 2007). Thomas (2007) studied faults within the approximately E-W-trending Grenadier fault block between the boundary of the Uncompahgre uplift and the Paradox basin, including the NW-SE striking Coal Bank Pass fault and E-W striking Snowdon fault (Figure 2). Thomas (2007) interpreted these faults to have been active during deposition of the Pennsylvanian Hermosa Group and to be overlapped by the Permian Cutler Formation; however, further investigation is needed to confirm this. The *en echelon* folding of Paleozoic strata adjacent to these faults suggest that these structures record sinistral slip or sinistral transpression (Thomas, 2007). This conclusion is compatible with an overall NE-SW shortening regime for the ARM system in this region. The Coal Bank Pass and Snowdon faults parallel contacts between the quartzite and phyllite layers of the Paleoproterozoic Uncompahgre Group that underlies the Paleozoic strata, suggesting preexisting structures in the Uncompahgre Group influenced ARM deformation (Thomas, 2007).

The deformation history of the ~1.7 Ga Uncompahgre Group is poorly constrained; however, in the Needle Mountains south of Ouray researchers have determined at least three deformational events occurred in the Paleoproterozoic through Mesoproterozoic (Karlstrom et al., 2017). These events were

contractional with N-directed and S-directed thrusting and folding associated with high-temperature, low-pressure contact metamorphism. Additional deformation may have that affected basement rocks prior to the ARM include possible Cambrian to Devonian age extension. Thomas (2007) determined that the Ignacio Quartzite was missing on the northern side of the Coal Bank Pass fault and the southern side of the Molas Creek fault zone. Given recent timing constraints on the Ignacio Quartzite to the Late Devonian (McBride, 2016), the relationship suggests that these faults were activate during Late Devonian extension prior to the deposition of the Elbert Formation.

This study focuses on the Ouray fault, located approximately 16 km south of the E-W-striking Ridgway fault, which is considered the primary boundary fault of the southwestern margin of the Uncompahgre uplift (Figure 2) (Stevenson and Baars, 1986; Thomas, 2007; Ewing, 2017). The Ridgeway fault cuts Mesozoic strata, offsetting the Jurassic Morrison Formation against the Cretaceous Mancos Formation, indicating that the fault was reactivated during the Laramide uplift (Thomas, 2007; Ewing, 2017). In the Ouray area, folded Proterozoic and Paleozoic strata adjacent to the Ouray fault are unconformably overlain by Triassic and younger stratigraphic units, which do not appear to be cut by the Ouray fault (Luedke and Burbank, 1962; Weimer, 1980; Burbank and Luedke, 2008; Ewing, 2017). The Ouray fault exposes the southern block of the steeply-dipping Uncompahgre Group (~1.7 Ga) and gently west-dipping Devonian strata, juxtaposing it with the northern block of exposed Mississippian and Pennsylvanian strata. The relationship between the Paleozoic and Triassic strata indicates that the Ouray fault is late Paleozoic in age and associated with the ARM. The lack of apparent displacement of the Mesozoic strata also indicates that the Ouray fault was not reactivated during the Laramide orogeny.

2.0 METHODS

In August 2020 we (Erinn Johnson and John Singleton) collected detailed structural data and performed geologic mapping in the area surrounding the Ouray fault. Structural data were collected using iPhones and the Stereonet Mobile application, and locations of all measurements and contacts encountered were recorded with a handheld GPS. Geologic mapping of the area was compiled based on >200 georeferenced observations and data collection sites (Plates 1 and 2). Petrographic sections from oriented samples of the Ouray fault were investigated for kinematics and deformation conditions, and one sample with calcite veins was analyzed via U-Pb laser ablation inductively-coupled plasma mass spectrometry (LA-ICP-MS) at the University of California-Santa Barbara.

2.1 Data Collection and Using Mobile Devices

Structural data were quickly and efficiently collected using the Stereonet Mobile application on iPhone versions 5 and 7. To reduce the error while using Stereonet Mobile and to determine representative mean orientations, we took multiple measurements of each fault and bedding surface. To further reduce the risk of error we regularly calibrated the phones against a Brunton compass and calibrated the magnetometer by rotating the phones in a figure-eight or circular motion (Allmendinger et al., 2017). For each measurement faults, bedding, joints, and veins were differentiated within the application. We limited our collection of faults to those with outcrop traces of over one meter. The sense of slip on fault planes were primarily determined using the R- and/or T-fracture criteria outlined in Petit (1987) or mineral slickenfiber steps (mostly calcite or chlorite).

The GPS in our mobile devices is not as accurate as a handheld GPS, so the handheld GPS was used as the primary basis for the locations provided in the geologic map. A waypoint was made for each outcrop where structural data were collected and/or where a mapping-related note was taken (Plate 1, Appendix A). All strike and dip measurements presented in this study are in the right-hand-rule convention written as strike, dip, dip quadrant, and lineation data are written as trend, plunge.

In addition to the location data, we recorded the Stereonet Mobile plane measurement number(s), an approximate average of the plane and lineation measurement(s) and the unit for each datum. When

collecting fault data specifically, we described the fault, including the kinematic indicators and interpreted sense of slip, a slip-sense confidence rating from 0 (no confidence) to 5 (completely confident), and the mineralization associated with the fault. A benefit of Stereonet Mobile is that it can simultaneously collect the planar data and linear data on a fault surface. Structural and GPS data were downloaded daily for backup and inspection on satellite imagery.

2.2 Data Organization

After returning from the field, I sorted and organized the data collected. The data exported from the Stereonet Mobile application is in a text file format which can be brought into Excel and split based on their type, with timestamps confirming matches between paired fault plane and slickenline lineation data. The naming system for the data is as follows: the GPS location (E# or J#), the plane number(s) (#_##), the plane type (B=bedding, BF = bedding-parallel fault, F = fault, J = joint, V = vein, VF = vein fault or vein with slickensided fault margin), and the geologist followed by the date (JSYYYYMMDD or EJYYYYMMDD). The final data set with averaged measurements is provided in Table A-1 (Appendix A).

To average structural measurements from an individual location, I used the “mplstereonet Package” program (2013) and Python script written by CSU graduate student M. Cole Sitar (2020). Once I formatted my data to work with the script, I was able to run my data through the program. The program automatically calculated the eigenvectors and eigenvalues for lineations and poles to planes, with the maximum eigenvector representing the mean orientation.

2.3 Graphical and Kinematic Analysis

For the kinematic analysis of the data, I used the graphical methods of Marrett and Allmendinger (1990) and the software programs Stereonet 11.2.2 and FaultKin 8.1 to evaluate the incremental shortening and extension directions (P- and T-axes, respectively) of the faults measured during this study (Marrett and Allmendinger, 1990; Allmendinger et al., 2012; Cardozo and Allmendinger, 2013). These paleostrain directions were used to assess kinematic compatibility of different fault populations and to determine overall kinematic patterns based on linked Bingham shortening and extension axes. The

method requires the record of the fault plane orientation, the orientation of the slip, and the slip sense – all of which make up a fault-slip datum.

While performing the analysis of the fault data, I split the faults up into different groups. One analysis evaluated fault patterns within certain distances of the Ouray fault (<10 m, 0–100 m, 100–200 m and >200 m). For each distance range, I plotted the fault planes and slickenlines, contoured P- and T-axes with the eigenvectors, and the fault plane solution based on the mean P- and T- axes (incremental shortening axis and incremental extension axis, respectively). This method of spatial organization is intended to identify the kinematics associated with the Ouray fault and relation to minor faulting in adjacent units. Similarly, I plotted faults separated by age (Paleoproterozoic vs. Paleozoic) and by the fault kinematics: normal, reverse, sinistral and dextral. Fault plane solutions were used to identify the dominant strain directions and overall kinematic pattern of the data. Within a small population of the data, the P- and T- axes plot in opposite quadrants of the fault plane solution, indicating kinematic incompatibility. In these cases, the outlier fault slip data were removed to create a kinematically-compatible fault plane solution model. All contours on the stereonet plots within this report are Kamb contoured with an interval of 2, a significance level of 2, 40 grid spacing, and smoothed.

Additionally, I performed graphical geometric analysis of the bedding planes, joints and vein orientations. The bedding planes were organized by each geologic era (Paleoproterozoic, Paleozoic, and Mesozoic units) and plotted separately with contours and cylindrical best-fits from eigenvectors to poles. Bedding measurements within 30 m of the Ouray fault were plotted to evaluate possible influence of Proterozoic bedding on fault orientation and to isolate folding of Paleozoic strata spatially associated with the fault.

The data were analyzed using the Vollmer (1990) classification of orientation data. This analysis involved calculating the eigenvectors in Stereonet, then calculating the P, G and R values of specific data sets to determine if they are classified as a point (P), girdle (G), or random (R) distribution, where $P = \lambda_1 - \lambda_2$, $G = 2(\lambda_2 - \lambda_3)$, and $R = 3\lambda_3$, and λ_1, λ_2, and λ_3 are the maximum, intermediate, and minimum eigenvalues, respectively (Vollmer, 1990).

2.4 Mapping

Mapping was performed in the field predominantly by collecting detailed georeferenced structural measurements and observations of structures and rock relationships. All measurements and observations were located using a Garmin 64st (version 4.60) unit. Preliminary mapping in the field was performed with the Touch GIS application on an iPad with cached high-resolution satellite imagery and previous published mapping of the region (Luedke and Burbank, 1962, 1981). Plate 1 contains all the GPS points taken while mapping the area. The map was digitized at 1:5,000 scale using ArcGIS, and finalized in Adobe Illustrator. In ArcMap, one-meter accuracy LiDAR data published in 2018 by the U.S. Geological Survey National Geospatial Program was converted in to a hillshade used as the basemap for the geologic map (Plate 2).

2.5 Calcite U-Pb Geochronology

Calcite veins from one oriented sample of the Ouray fault principal slip plane were analyzed using U-Pb LA-ICP-MS at the University of California-Santa Barbara. Calcite U-Pb LA-ICP-MS dating within the last 10 years has become a widely used geochronological method (e.g., Roberts et al., 2020). This method has proven to be particularly useful for dating veins and faults with synkinematic calcite (e.g., Roberts and Walker, 2016; Ring and Gerdes, 2016; Nuriel et al., 2017, 2019; Miranda et al. 2020; Roberts et al., 2021). A limitation of this method is that calcite commonly does not have enough uranium to provide meaningful ages.

Dr. Andrew Kylander-Clark at the UC-Santa Barbara LA-ICP-MS lab performed the analysis on a thick section from the principal slip plane of the Ouray fault using instrumentation and standards outlined in Kylander-Clark (2020) and Nuriel et al. (2021). The thick section contains zones of calcite mineralization that were targeted for the study. A total of 50 spots were analyzed with a spot diameter of 110 µm (Appendix A, Table A-3). Given that calcite typically has a significant component of common lead, the sample date was determined via Tera-Wasserburg diagram lower intercept. Using the Tera-Wasserburg method accounts for the affects that the common lead (non-radiogenic) has on U/Pb ratios.

3.0 DATA AND OBSERVATIONS

3.1 Map Relationships and Folding

The units surrounding the Ouray fault include the Paleoproterozoic Uncompahgre Group and the Paleozoic Elbert Formation (Devonian), Ouray Limestone (Devonian), Leadville Limestone (Mississippian), Molas Formation (Mississippian-Pennsylvanian), Hermosa Group (Pennsylvanian), and Cutler Formation (Permian). The Mesozoic units consist of the Dolores Formation (Triassic) and the Entrada Sandstone (Jurassic). There are four unconformities within this stratigraphic section, the oldest of which is the contact between the Paleoproterozoic Uncompahgre Group and the Late Devonian Elbert Formation. This contact is termed the “Great Unconformity”, which consists of both a nonconformity and angular unconformity spanning approximately 1.3 billion years (Figure 3). Bedding in the Uncompahgre Group below the unconformity is typically subvertical, whereas Devonian strata dip gently, indicating that significant folding in Uncompahgre Group predated Devonian deposition, most likely occurring during 1.7 to 1.4 Ga shortening (Karlstrom et al., 2017). We found evidence of faulting pre-Elbert Formation at Box Canyon where an apparent reverse fault cuts the Uncompahgre Group but terminates at the Great Unconformity contact (Figure 3).

The other unconformities include a disconformity between the Leadville Limestone and the Molas Formation, and an angular unconformity between the Permian Cutler and Triassic Dolores Formations (Figure 3). This angular unconformity is particularly evident in the region because the Dolores Formation transgresses the Cutler Formation and locally overlies the Hermosa Formation (Figure 3, Figure 4) (Luedke and Burbank, 1962). The most recent unconformity occurs where the Oligocene San Juan Formation overlies units ranging from the Paleoproterozoic Uncompahgre Group up to the Cretaceous Mancos Shale (Figure 3) (Luedke and Burbank, 1962).

The 2.5 km-thick Uncompahgre Group (~1.7 Ga) is dominated by quartzite with layers of slate/phyllite. In the Ouray region this group has subvertical bedding (Figure 3, Figure 5) and is intensely folded from multiple Proterozoic deformation events (Karlstrom et al., 2017). We mapped two sets of tight to isoclinal anticlines and synclines (Plate 2; Figure 6). The WNW-ENE-trending anticline mapped closest to the Ouray fault is upright with near vertical to overturned limbs (Plate 2). The Uncompahgre quartzite

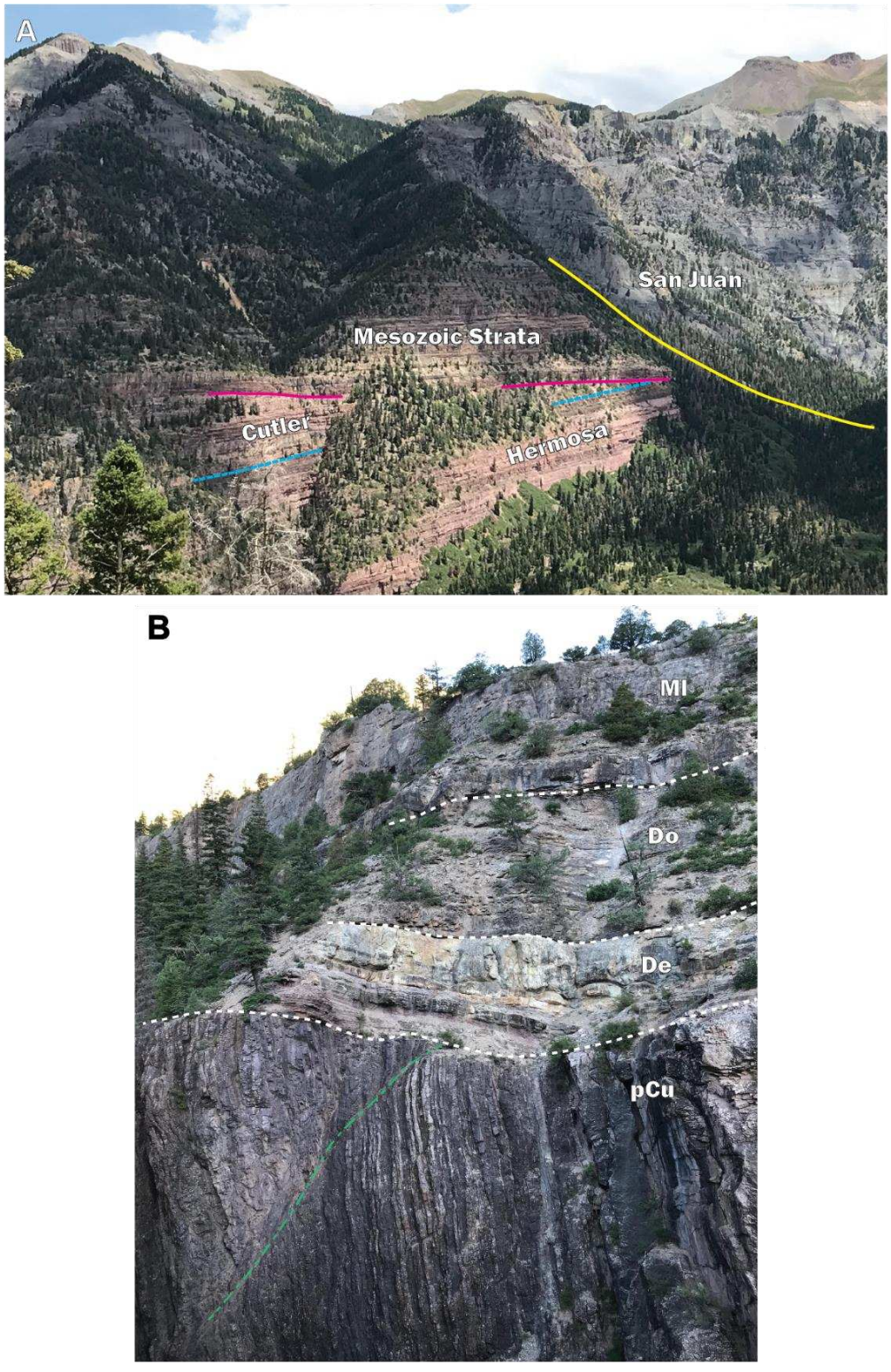

Figure 3. Annotated photographs of unconformities and map relationships. A) The relationship between the Hermosa Group and Cutler Formation (blue dashed contact) with the angular unconformity at the Dolores Formation (pink contact) and younger Mesozoic units. And the nonconformity of the San Juan Formation overlying the Pennsylvanian through Mesozoic strata (yellow contact). B) The Great Unconformity at Box Canyon; the green dashed line is a pre-Elbert Formation fault. pCu = Uncompahgre Group, De = Elbert Formation, Do = Ouray Limestone, Ml = Leadville Limestone

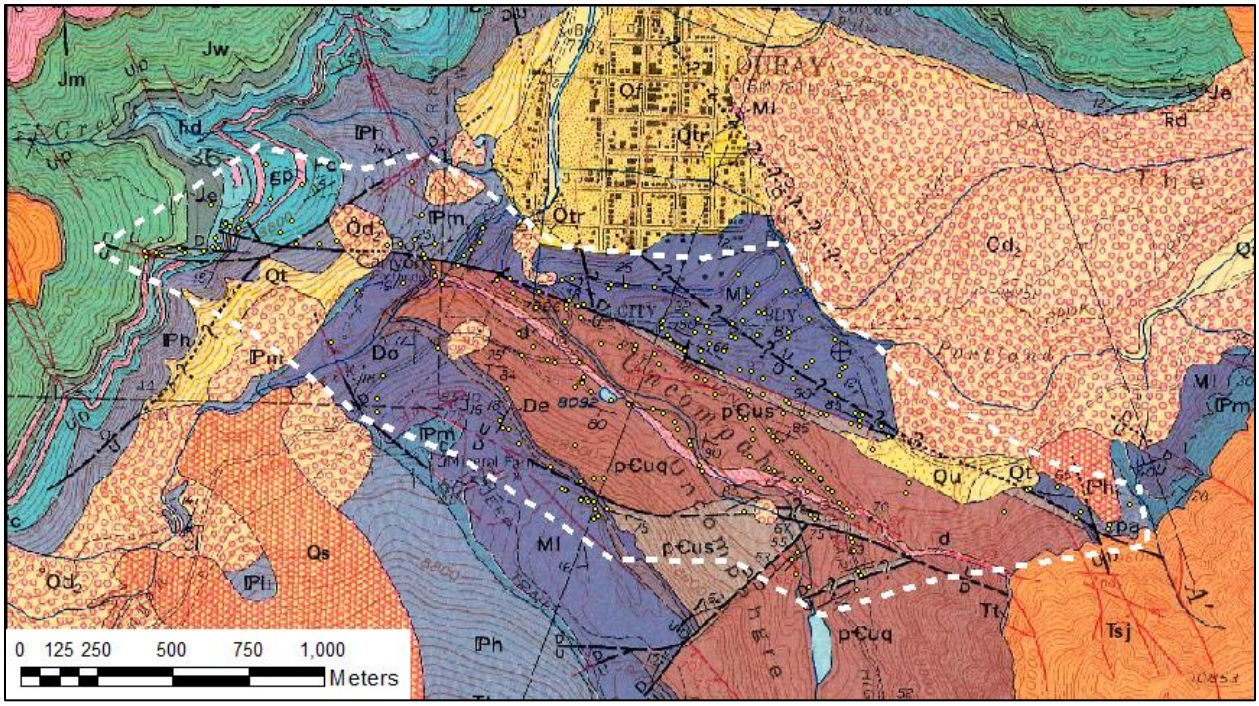

Figure 4. A portion of the Luedke and Burbank (1962) geologic map of the Ouray quadrangle (GQ-152) shown with the GPS points in yellow (Plate 1) and the mapping area outline in white (Plate 2).

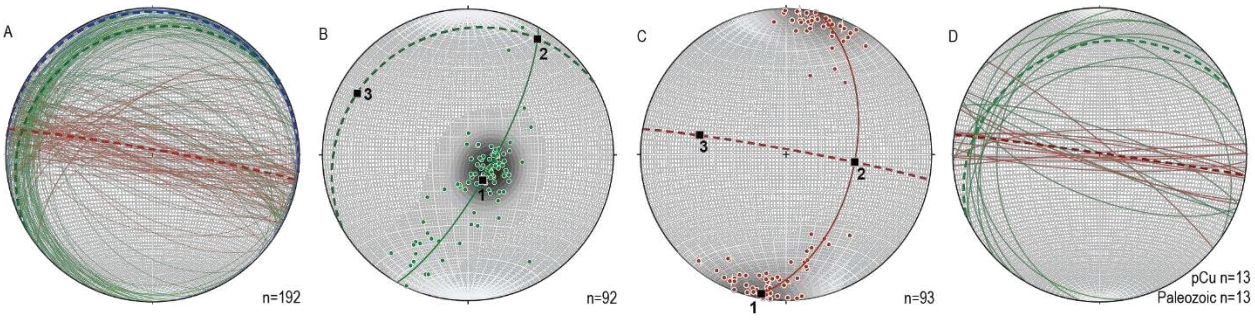

Figure 5. Stereonet plots of bedding planes within the vicinity of the Ouray fault. (A) All bedding planes; Proterozoic bedding planes are red (mean plane orientation in bold = 280/87°N), Paleozoic bedding planes are green (mean plane = 240/16°N), Mesozoic bedding planes are blue (main plane = 277/3°N) (B) Paleozoic bedding poles contoured. Maximum eigenvector = 150,74°, best fit great circle 029/76°E, minimum eigenvector (fold axis) = 299/14° and mean plane = 240/16°N. (C) Uncompahgre Group bedding poles contoured. Maximum eigenvector = 184,87°, best fit great circle 013/51°E, minimum eigenvector (fold axis) = 283/39° and mean plane = 280/87°N. (D) Bedding planes within 30 m of the Ouray fault. Paleozoic mean plane = 246/26°N, and Proterozoic mean plane = 278/89°N.

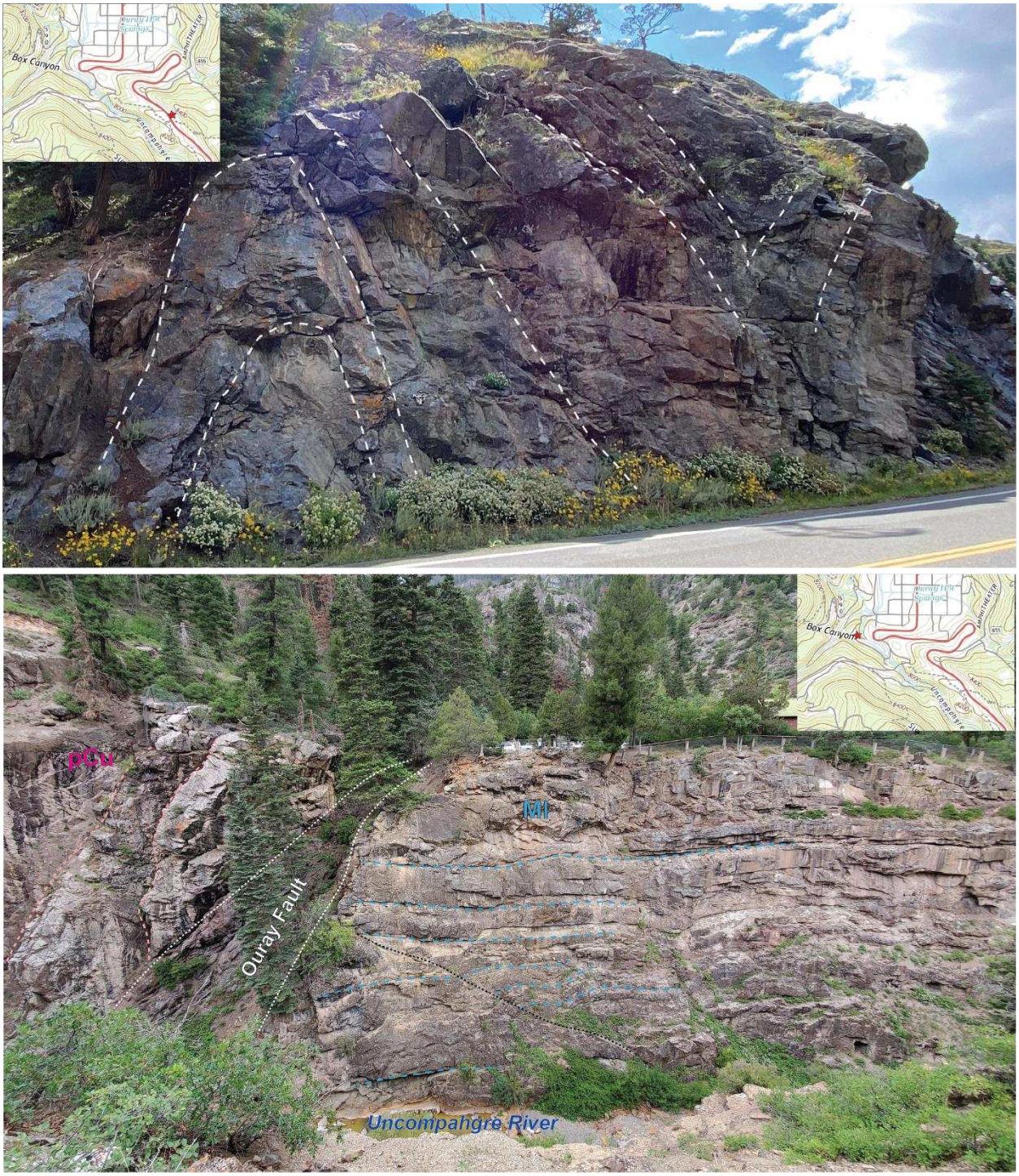

Figure 6. Outcrop photographs of Uncompahgre Group folds and the Ouray fault. (Top) Tightly- to isoclinally-folded Uncompahgre quartzite along a Highway 550 roadcut (photo by Morley Beckman). (Bottom) The Ouray fault below the Box Canyon parking lot (view is looking to the west). Denoted in pink on the left (south) is the subvertically-oriented Proterozoic Uncompahgre quartzite (pCu), which is cut by the Ouray fault, denoted in white. Denoted in blue to the north of the Ouray fault is the Mississippian Leadville Limestone (Ml). The dotted black line in this unit is an apparent N-dipping thrust fault.

has retained its original cross bedding, allowing us to determine the stratigraphic younging directions in some locations.

The 9- to 15-meter-thick Elbert Formation unconformably overlies the Uncompahgre Group and gradually grades into the younger Ouray Limestone (Figure 3b). The 18- to 22-meter-thick Ouray Limestone beds also gradually grade into the massive Mississippian Leadville Limestone (55–72 m thick) (Burbank and Luedke, 2008). At Box Canyon (Perimeter Trail), these units primarily dip shallowly west but form a monocline along the S-side of the Ouray fault with a fold axis that trends <40° from the fault trace (Figure 7, Plate 2).

The ~2.5 km long Ouray fault trends ESE-WNW south of the town of Ouray. The fault splits the geologic units in the area into a northern and southern block with S-side-up apparent displacement. The northern block primarily consists of exposed Leadville Limestone and younger strata, whereas the southern block exposes the Uncompahgre Group and Devonian units (Figure 3, Figure 8). At the easternmost exposure of the Ouray fault, the juxtaposed Uncompahgre Group and Leadville Limestone are overlapped by the San Juan Formation. At the western end, the fault has placed the Uncompahgre Group and overlying Devonian units adjacent to the Hermosa Group. During our field work we found no evidence of the Ouray fault extending into the Permian Cutler Formation or Mesozoic strata. Prior mapping by Luedke and Burbank (1962, 1981) shows the fault continuing WNW into the Mesozoic strata with little to no displacement (Figure 4).

The Leadville Limestone dips gently 10° to 30° W in the southern block of the Ouray fault. This general orientation continues on the northern block at Box Canyon (Figure 6b). However, along the east-central part of the Ouray fault the Leadville Limestone in the northern block is folded into a tight to open NNW- to NW-trending syncline (Figure 9; Plate 2). This syncline was previously mapped as a fault by Luedke and Burbank (1962, 1981) (Figure 4); however, we did not observe evidence of a NW-trending fault at this location. The syncline axial trace nearest to the Ouray fault parallels the fault with the tightest interlimb angle at ~49° and bedding slightly overturned next to the fault – east of cross section A-A' (Figure 9; Plate 2). Moving west the fold opens up, and the axial trace turns approximately 45° away from the fault then turns back towards parallelism with the fault again, where the tightest interlimb angle is

~106°. The northwestern limb of this fold has gently-dipping bedding almost to the point of being monoclinal (Figure 9; Plate 2).

The Pennsylvanian Hermosa Group and Permian Cutler Formation form an angular unconformity with the overlying Triassic Dolores Formation (Figure 3a). The Paleozoic strata generally dip ~10 to 30° to the NW, where the Mesozoic strata dip from 2 to 10° to the N (Figure 5, Plate 2). In Figure 3a, the angular unconformity can be seen where the Cutler Formation is erosionally cut out, and the Dolores Formation overlies the older Hermosa Group.

The Cutler Formation and Mesozoic units (Triassic Dolores Formation and Jurassic Entrada Sandstone) are intruded by porphyritic granodiorite sills of Laramide age (Late Cretaceous and Paleocene/early Eocene). Overlying these units is the propylitically-altered Oligocene San Juan Formation of volcanic tuffs, flow breccias, and lava flows spread across the region through paleovalleys and over ridges, resulting in highly variable thicknesses of the unit (Figure 3a; Plate 2).

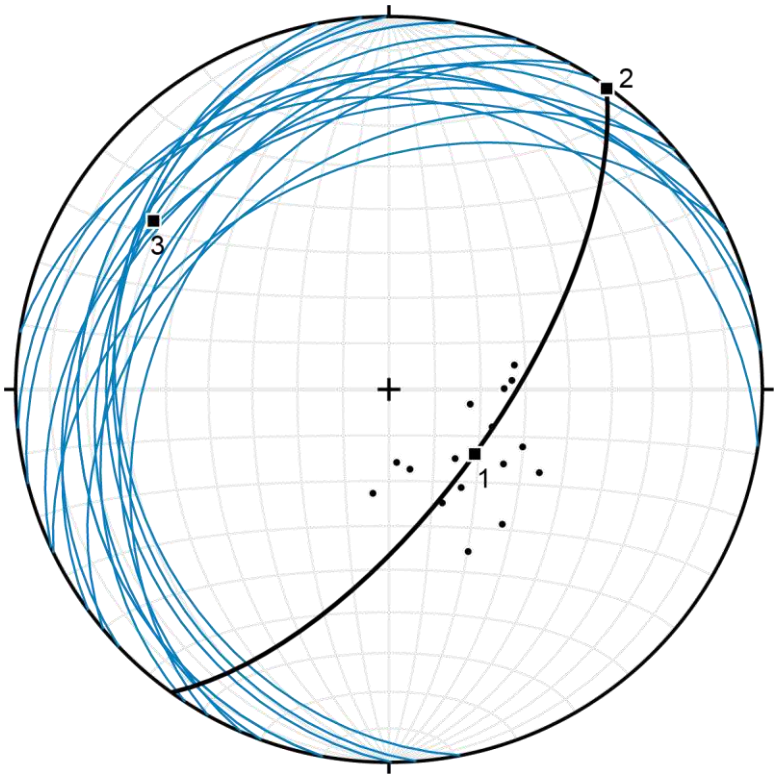

Figure 7. Bedding in Paleozoic strata involved in monoclinal folding adjacent to the Ouray fault near Box Canyon. Bedding planes (blue) with the steepest dipping bed at 244/40°N. The cylindrical best fit plane (black) is oriented 036/67°W.

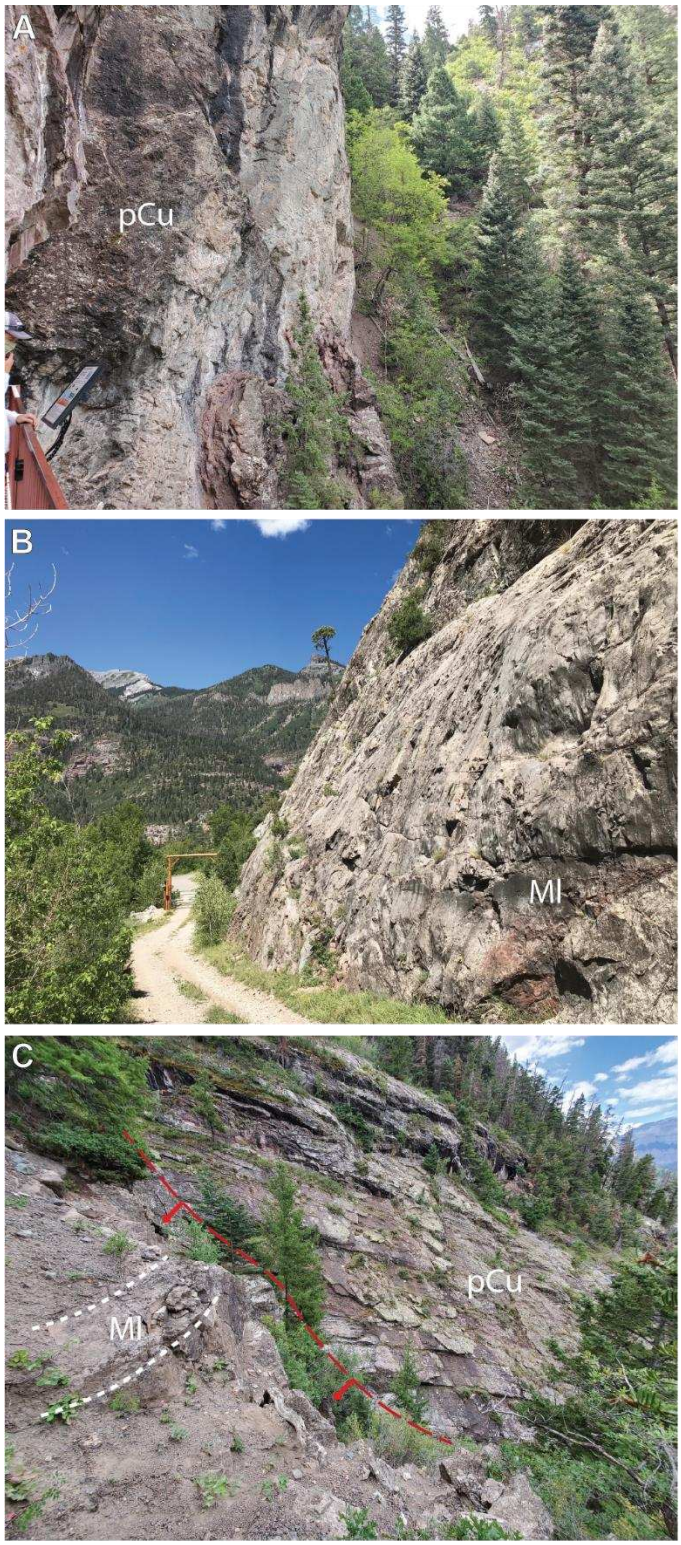

Figure 8. Photographs of the Ouray fault outcrops organized from west to east. A) Ouray fault at Box Canyon with Uncompahgre Group quartzite on the left (S side) and Paleozoic strata hidden by vegitation on the right (N side). B) Ouray fault principal slip plane on the Leadville Limestone dipping steeply S off of HWY 550. C) Ouray fault at the southeastern most extent of the map area red dashed line delineates the fault contact in the valley below. pCu = Uncompahgre Group, Ml = Leadville Limestone.

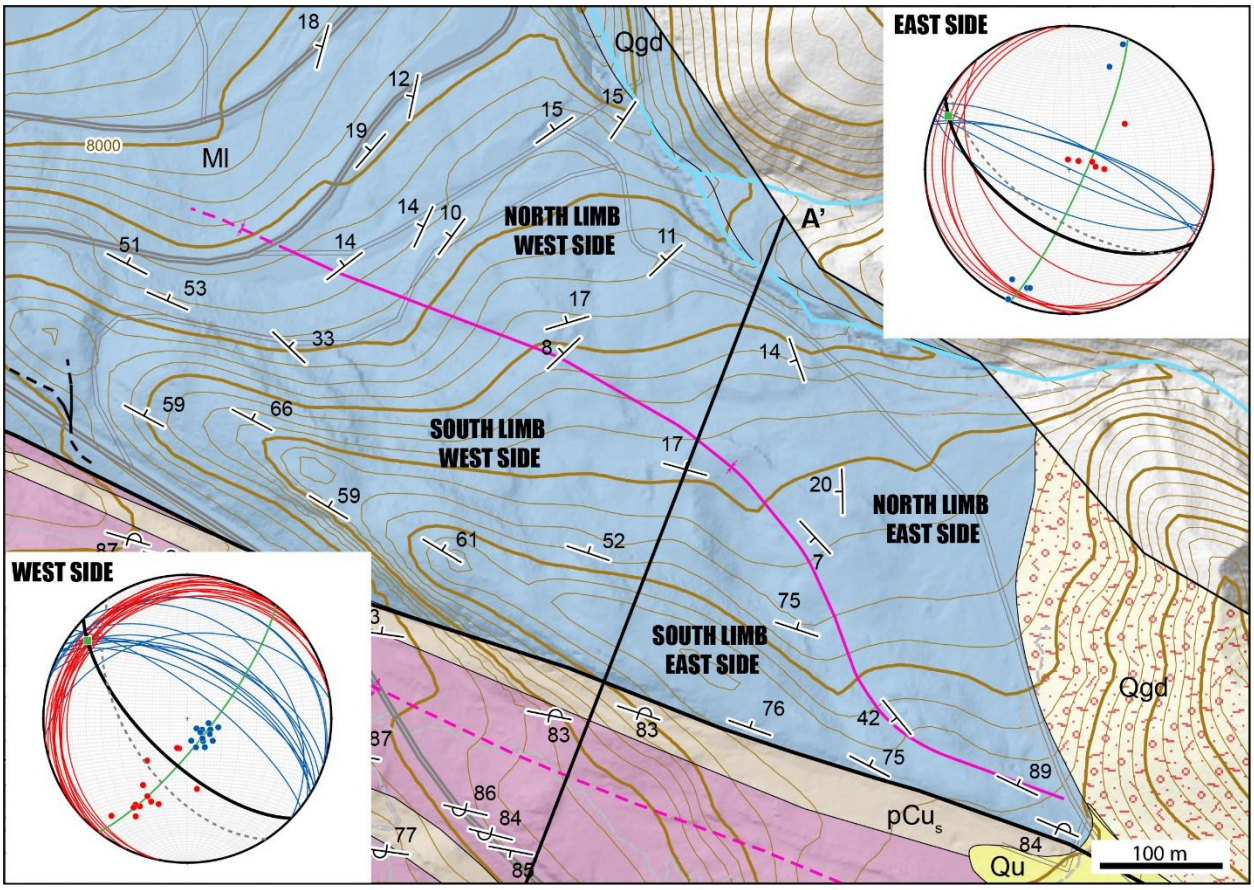

Figure 9. Mapped syncline in the Leadville Limestone (after Plate 2). Bedding planes on the north limb of the syncline are red on the stereonet plots; the south limbs are blue. The solid black line is the approximate axial plane of each fold. The west side axial plane is oriented 134/66°S with an average interlimb angle of 134°. The cylindrical best fit plane and fold axis are oriented 038/77°W, and 308,13°, respectively (in green). The east side axial plane is oriented 121/55°S with an average interlimb angle of 85°. The cylindrical best fit plane and fold axis are oriented 024/81°W, and 294, 9°, respectively (in green). Dashed in gray are the axial planes based on the steepest limb measurements. The west side steepest axial plane is oriented 147/56°W with the tightest interlimb angle of 106°. The east side steepest axial plane 124/62°S with the tightest interlimb angle of 49°.

3.2 Faults in the Uncompahgre Group and Paleozoic Strata

The primary fault slip sense indicators in the Uncompahgre Group are chlorite or quartz mineral fiber steps, with the occasional R-shear, T-fracture or offset marker (Figure 10). However, many of the faults are coated with chlorite or iron oxide with no clear sense of slip indicators. The slip sense indicators of Paleozoic faults, specifically in the Leadville Limestone and the Hermosa Formation, are typically clearer and commonly indicated by calcite slickenfiber steps (Figure 10) with less common R-shears, oblique gouge fabric, and offset markers. We determined a slip sense on 55% of faults in the Uncompahgre Group and 64% of faults in the Paleozoic units (Figure 11).

Figure 10. Fault surface feature photographs. A) John Singleton measuring a fault plane in the Leadville Limestone using the Stereonet Mobile App off of HWY 550. B) Example of well formed calcite slickenfiber steps on a Leadville Limestone fault indicating dextral slip. C) Calcite slickenfiber steps on a south-dipping fault in the Leadville Limestone with oblique reverse/left-lateral slip. D) Chlorite slickenfiber steps on the Uncompahgre Group indicating sinistral slip.

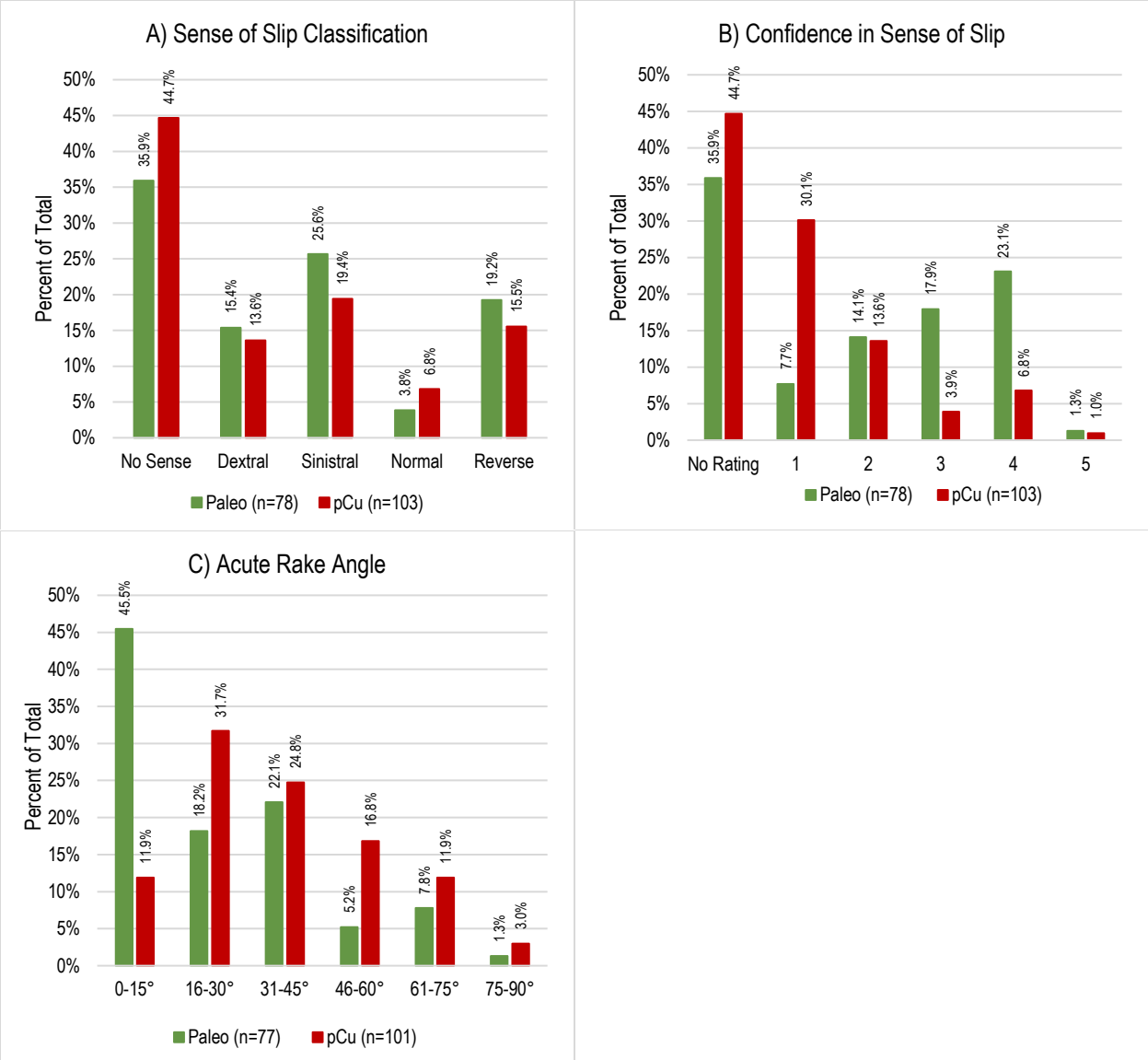

Figure 11. Histograms of the fault data in Paleozoic and Proterozoic units. A) Fault sense of slip classification. B) Confidence rating of the sense of slip ranging from 0-5 (no confidence to extremely confident). C) Angles of the acute slickenline rake.

The dominant fault orientation dips steeply to the south, with a mean plane of 108/80°S. The Uncompahgre Group faults are more steeply dipping than faults in the Paleozoic strata, with average planes oriented ~108/88°S and ~105/69°S, respectively (Figure 12). The Uncompahgre Group shortening direction (P-axes) trends subhorizontally to the NE-SW, accommodated by a dominant sinistral slip with minor amounts of oblique reverse influence (Figure 12). Within the Paleozoic strata the shortening direction remains subhorizontal NE-SW. Contrary to the Uncompahgre Group, the Paleozoic strata accommodates mostly reverse slip with sinistral influence (Figure 12).

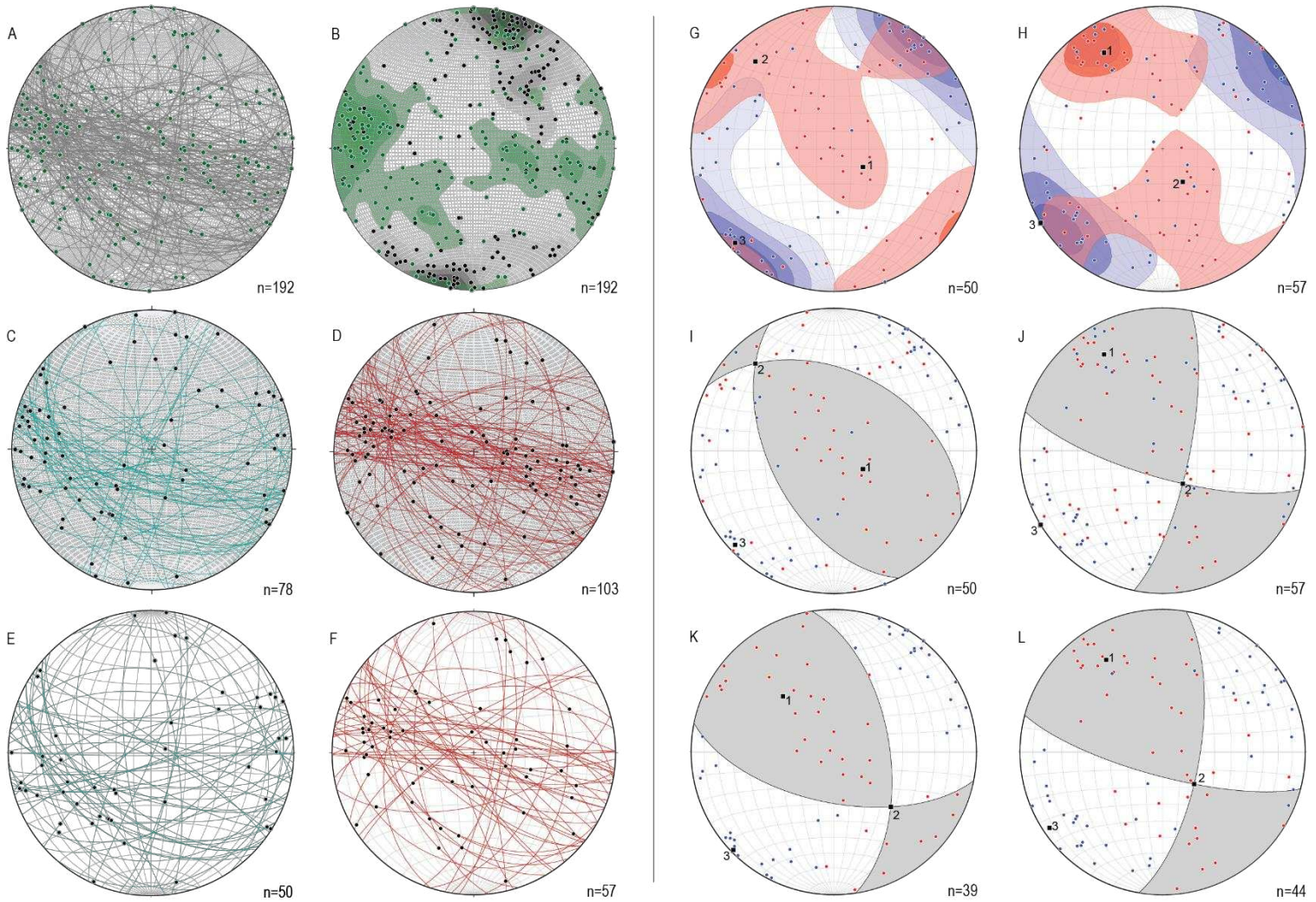

Figure 12. Stereonet plots of fault data. A) All measured fault planes and their slickenline orientations. B) A contoured stereonet of the slickenlines (green) and poles (black) for all the faults. C) All measured Paleozoic fault plane and slickenline measurements. D) All measured Paleoproterozoic fault and slickenline measurements. E) All measured Paleozoic faults and slickenlines with a sense of slip. F) All the Paleoproterozoic faults and slickenlines with a sense of slip. G) Contoured P- and T-axes (blue and red, respectively) for the Paleozoic faults. H) Contoured P- and T-axes for the Paleoproterozoic faults. I) Fault plane solution of the Paleozoic faults with linked Bingham axes. J) Fault plane solution of the Paleoproterozoic faults with linked Bingham axes. K) Modeled fault plane solution of the Paleozoic faults with outlier fault data removed. L) Modeled fault plane solution of the Paleoproterozoic faults with outlier fault data removed.

A large portion (46%) of the Uncompahgre Group faults we measured are parallel or subparallel to bedding, whereas in Paleozoic faults only one measured fault parallels bedding. Bedding-parallel faults in the Uncompahgre Group are mostly subvertical (Figure 5). Measured bedding planes in the Uncompahgre Group have a mean orientation of 280/87°N, whereas the faults have a mean orientation of 108/88°S, only ~9° apart. By contrast, the Paleozoic average bedding plane orientation is 240/16°NW, and the average fault orientation is 103/70°S (~80° difference). The geometric relationship between the Uncompahgre Group bedding and faults indicates that the Proterozoic subvertical folding exerted significant influence on brittle fault geometry. The faults in the Paleozoic strata were less affected by preexisting folding and anisotropy.

Slickenline lineations commonly rake less than 45° in all rock units, the mean orientation of all the slickenlines is 272, 13° (Figure 11c, Figure 12). A majority of the Paleozoic strata slickenlines rake ≤15° (46%) and have a mean orientation of 262, 13°. The Uncompahgre Group has a smaller majority of slickenlines raking 16–30° (32%) and having a mean orientation of 279, 5°. These trends indicate strike-slip movement was dominant. On a couple occasions, we discovered multiple sets of slickenfiber orientations both in the Uncompahgre Group and in the Leadville Limestone, indicating multiple slip events on those surfaces had occurred.

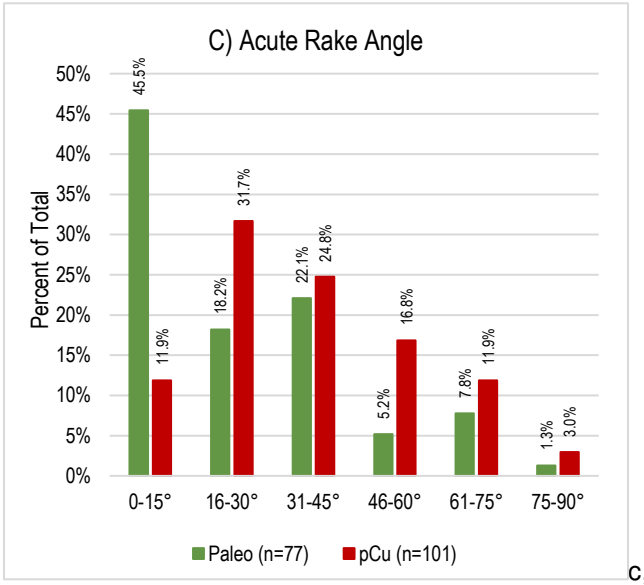

Plotting all the fault data from Paleozoic and Proterozoic units by slip type (i.e., normal, reverse, dextral, sinistral) indicates dominant reverse and sinistral slip in the region (Figure 11, Figure 13). Fault plane solutions indicate that the reverse and sinistral faults record nearly equal NE-SW directed

shortening directions (Figure 14). The reverse faults record subvertical extension, whereas the sinistral faults record NW-SE extension, and together they define a subvertical NW-striking plane of extensional axes, perpendicular to the dominant shortening direction. The normal faults indicate a subhorizontal NE-SW directed extension with subvertical shortening, which is clearly incompatible with the reverse faults. The dextral faults, when using the “raw” fault plane solution, indicate subhorizontal ~E-W shortening with subvertical extension, yielding a reverse fault regime fault plane solution. When using the modeled fault plane solution, where the incompatible P- and T- axes were removed, the shortening direction remains ~E-W; however, the mean extension direction is oriented ~N-S with a strike-slip fault plane solution (Figure 14).

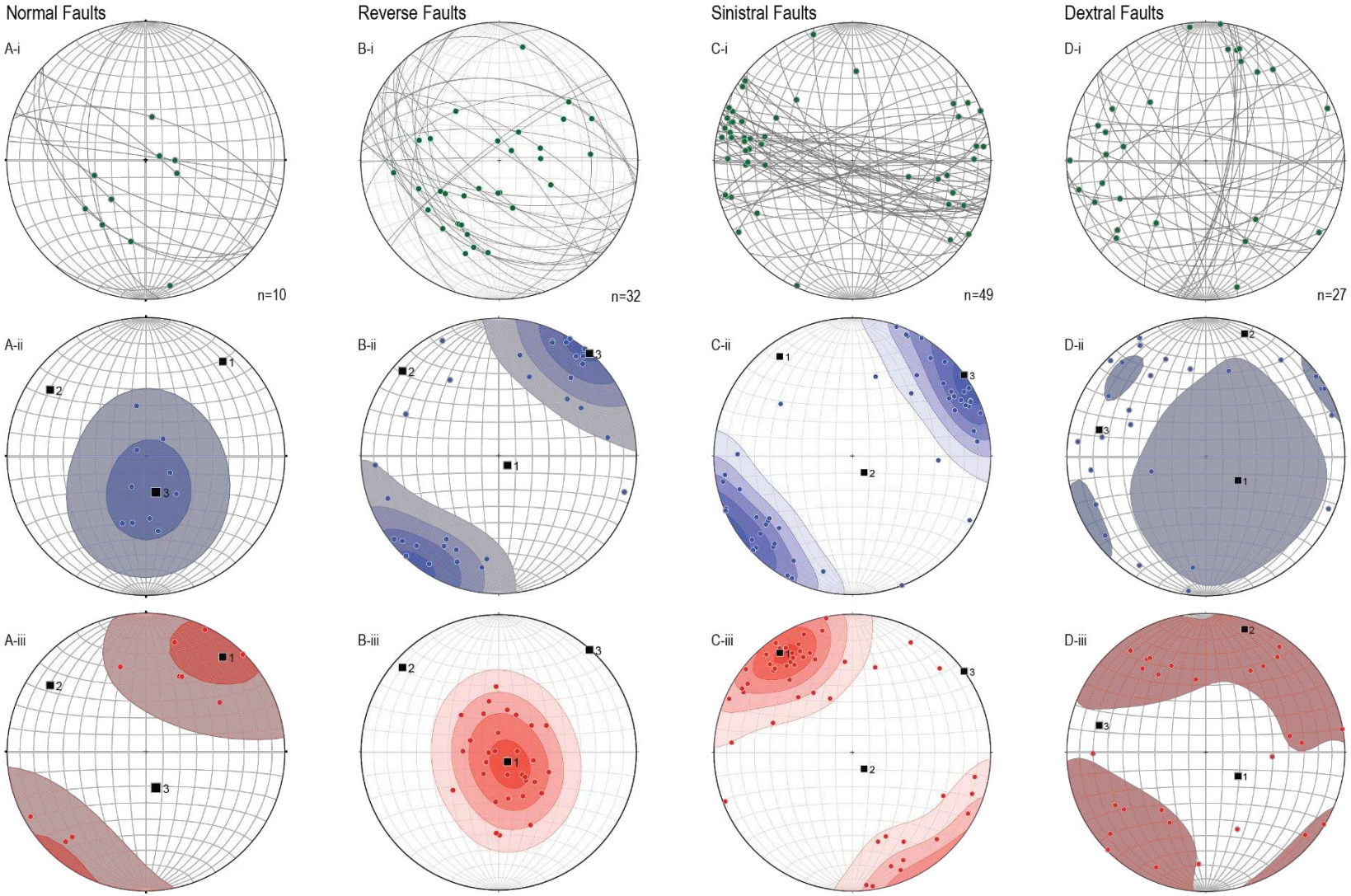

Figure 13. Fault kinematic data separated by the fault type. Column A are the normal faults, column B are the reverse faults, column C are the sinistral faults and column D are the dextral faults. Row “i” displays the fault planes and fault surface lineations (green) with sense of slip. Row “ii” displays the contoured P-axes and their eigenvectors. Row “iii” displays the T-axes and their eigenvectors. These are Kamb contoured with an interval of 2, a significance level of 2, and 40 grid spacing. The fault plane solutions for these faults are shown in Figure 14.

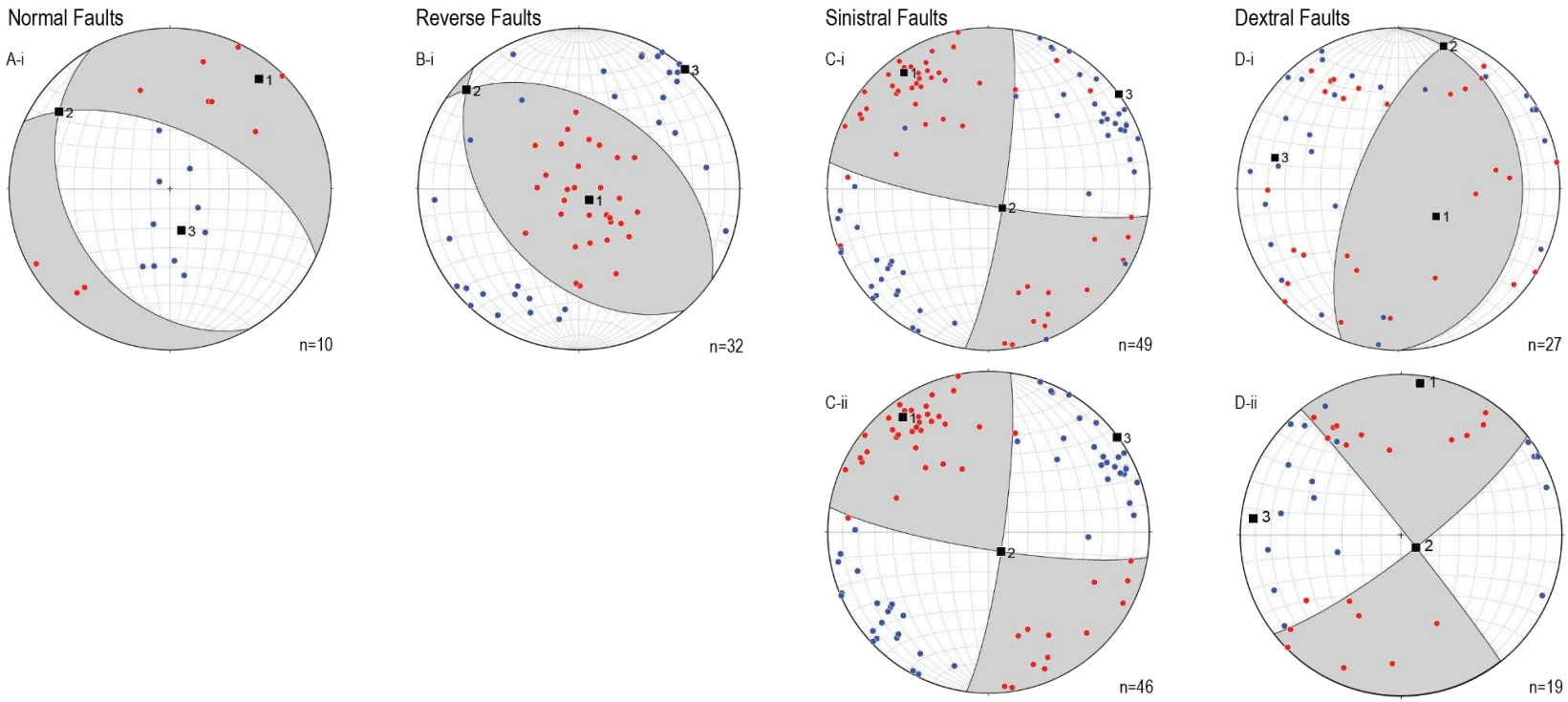

Figure 14. Fault plane solutions of the fault data by fault type. The “i” stereonet plots are all of the original data, where the “ii” are the corrected fault plane solutions. The correction was made by removing all the P and T axes where both points were in the incompatible zone of the solution. The normal and reverse faults did not meet the qualifications for correction.

3.3 Ouray Fault

The ESE-WNW trending Ouray fault exposure spans approximately 2.5 km south of the town of Ouray. The fault generally dips between 90° and 70° to the south. The best exposures of the Ouray fault are west of Highway 550 at Box Canyon, and about 300 m south on Highway 550 from the start of the switchbacks into the town of Ouray (Plate 1: GPS points E151 and E56-E57, respectively, Figure 8a & b). At Box Canyon the vertical displacement based on separation of Paleozoic strata is estimated to be 165 ± 10 m of S-side up movement (Plate 2, B-B'). However, the slickenline data collected on the principal slip plane indicate primarily strike-slip movement of the Ouray fault (Figure 15). The slickenline data collected within 10 m of the Ouray fault primarily plunge 4° to 37° WNW, with a couple of outliers at 164, 61°, 098, 31° and 086, 31°. None of the sense of slip indicators from the principal slip plane were conclusive; however, we assumed a sinistral slip sense based on the dominant WNW-plunging slickenline orientations and the apparent S-side up offset across the fault. This assumption is also supported by a majority of the subsidiary faults within ~30 m of the Ouray fault recording sinistral and/or reverse slip indicators.

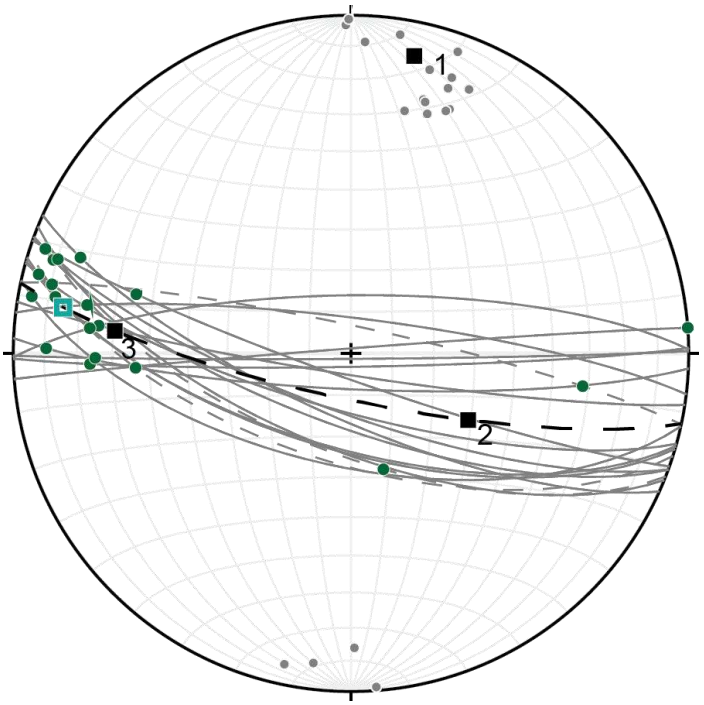

Figure 15. All faults within 10 m of and including the Ouray fault. The solid gray lines are the principal slip plane measurements where the dashed gray lines are the faults within 10 m of the fault but not on the principal slip plane. The mean plane of the Ouray fault and is 102/79°S (black dashed line) including all faults within 10 m. The green points are the slickenline orientations and the gray points are the poles to the planes. The maximum eigenvector of the poles is 012,11° and is a point distribution (P=0.876) under the Vollmer (1990) classification. The maximum eigenvector of the slickenlines is 279,14° (teal square) and is a point distribution (P=0.767).

At the two best exposures of the Ouray fault, the orientation of the principal slip plane varies, steepening to subvertical at Box Canyon. The mean orientations of the principal slip plane at Box Canyon (E151, Plate 1) and where it crosses Highway 550 (E056-E057, Plate 1) to the east are 273/89°N and 108/70°S, respectively. By combining all the principal slip plane measurements, the mean orientation of the Ouray fault plane is 101/80°S, with a mean slickenline orientation of 280, 15° (n=16) (these values change by ±1° when including subsidiary faults within 10 m of the Ouray fault (n=19)) (Figure 15). Using the mean orientation of the principal-slip plane and the mean slickenline orientation, the sinistral oblique slip displacement required to achieve 165 ± 10 m of S-side up vertical displacement is 647 ± 40 m. Burbank and Luedke (2008) interpret 600–700 ft (182–213 m) of S-side-up vertical displacement across the fault. Using these vertical displacement values and the average slickenline orientation from our data, the total sinistral oblique displacement is 714–826 m. These calculations suggest that the Ouray fault records ~600–800 m of oblique sinistral slip with a component of S-side up (high-angle reverse) slip.

The Ouray fault's influence on minor faulting in the surrounding rocks can be seen in Figure 16 where the faults have been plotted based on their distance from the principal slip plane. The data within 10 m of the Ouray fault have a mean orientation of 102/79°S and classify as a point distribution (P=0.876 for poles to faults). At 0–100 m the faults have a mean orientation of 106/73°S and classify as a point distribution, but with greater variability (P=0.519). At 100–200 m the data do not have a clear distribution pattern (P=0.348, G=0.341, R=0.311), and at greater than 200 m from the Ouray fault the data classify as random distribution (R=0.520). At 100–200 m the mean orientation of the faults is 278/83°N and at >200 m the mean orientation is 119/79°S.

The Ouray fault and adjacent subsidiary faults dominantly record NE-SW subhorizontal shortening and NW-SE extension (Figure 16a). Sinistral slip with a minor amount of reverse slip (sinistral transpression) is evident in the fault plane solution for faults within 10 m of the Ouray fault (Figure 16a). Expanding the data to include faults within 100 m, small-scale faults retain the NE-SW subhorizontal shortening with NW-SE extension directions and an overall sinistral transpression slip pattern (Figure 16b). Extending further out, between 100 m and 200 m from the Ouray fault, the NE-SW directed shortening pattern continues with sinistral transpression (Figure 16c). At over 200 m from the Ouray fault NE-SW shortening is still evident; however, these faults are more dominated by reverse slip than sinistral.

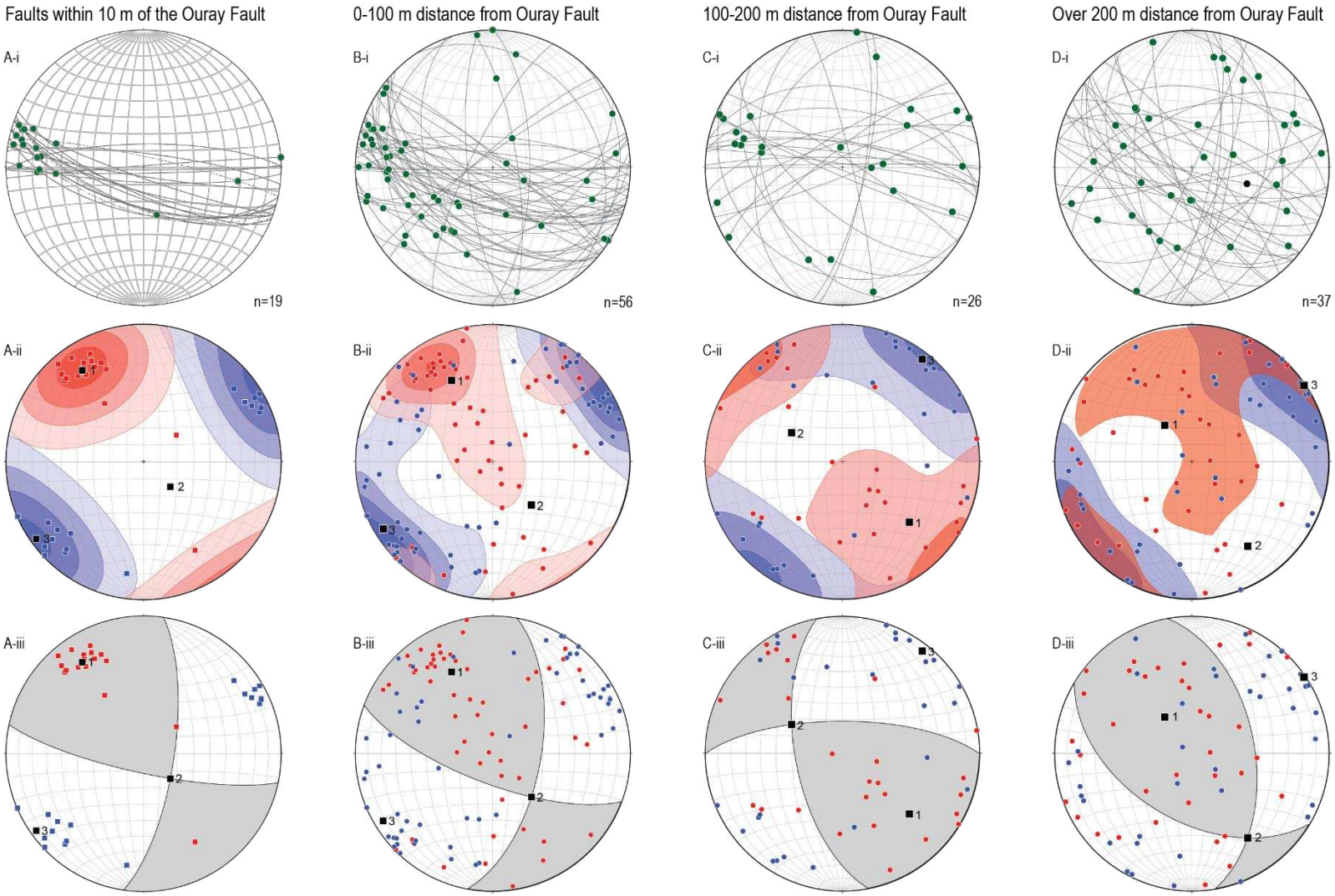

Figure 16. Fault kinematic data at varying distances from the Ouray fault. A-i through A-iii are data within 10 m of the Ouray fault. B-i through B-iii are data within 100 m of the Ouray fault. C-i through C-iii are data 100–200 m away from the Ouray fault. D-i through D-iii are data over 200 m away from the Ouray fault. Row "i" displays the fault planes and slickenlines (green). For A-i the dashed lines are the faults within 10 m but are not the Ouray fault itself (see Figure 15 for more detail). Row "ii" are the contoured P and T-axes of the faults with their eigenvectors. Row "iii" are the fault plane solutions of the data also plotted with their eigenvectors (linked Bingham axes).

Oriented petrographic sections from the principal slip plane of the Ouray fault in the Leadville Limestone west of Highway 550 record cataclastic textures (Figure 17). The grain sizes within these samples range from ~2.5 mm down to an aphanitic calcite groundmass. None of the samples show evidence of crystal-plastic flow or dynamic recrystallization, indicating only brittle deformation took place during the movement of the Ouray fault. Fine-grained opaque seams with irregular traces are present throughout all the sections, most likely recording dissolution-precipitation creep.

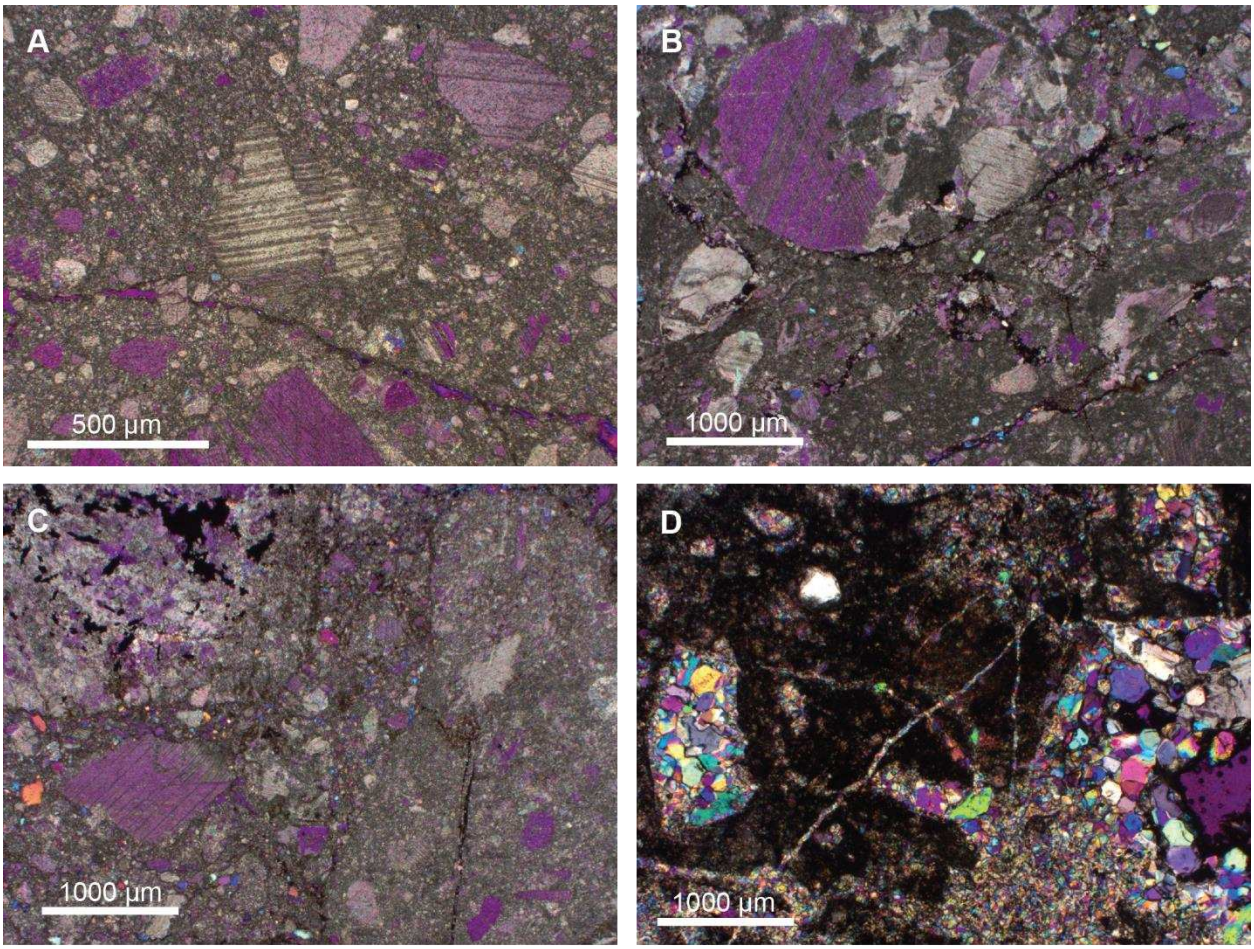

Figure 17. Photomicrographs of the oriented petrographic sections taken from the principal slip plane of the Ouray fault on the Leadville Limestone (Note: photos were taken in cross polarized light). A) E56b cataclasite with domino structure in calcite with offset twins (5x). Section cut perpendicular to the fault along slickenline rake (10°W). B) E57 cataclasite with twinned calcite and dark dissolution seams. Section cut parallel to strike (2.5x). C) E57b cataclasite with bent calcite twins. Cut along rake (18°W) (2.5x). D) E56c blobs of recrystallized quartz in an iron-oxide matrix derived from the Uncompahgre Group (thick section). Section cut subparallel to strike. Also see Figure 18a (2.5x).

3.3.1 Calcite U-Pb Geochronology Results

Fifty laser ablation spots were analyzed on thin (<2 mm) calcite veins from a sample of Leadville Limestone cataclasite along the principal slip plane of the Ouray fault. The analyzed calcite veins appear to be discontinuous fragments within cataclasite. Of these 50 laser-ablation spots, only six contained enough U to provide any results (3.3 to 17 ppm U) (Figure 18). The other 44 analyses contained less than 0.07 ppm U. Five of the six spots are located in the central calcite blob (~0.7 mm) (Figure 18). The sixth spot is located in the largest calcite blob (~1 mm wide, right) where none of the other spots contained sufficient U (Figure 18).

Using a Tera-Wasserburg concordia diagram linear regression of the six spots containing U, the lower intercept age was determined to be 39.3 ± 6.2 Ma (Figure 18). The relatively large error stems from the small sample size and the lack of data nearing the lower intercept (with higher U and radiogenic Pb). However, the mean square of weighted deviates (MSWD) value of 1.9 is low, suggesting one population of calcite ages.

The six U-rich spots that yield the late Eocene date are all adjacent to one another and located within a fragmented calcite vein surrounded by dark, very fine-grained matrix that locally includes a very thin (~20 µm) calcite veinlet that cuts across the fine-grained matrix, suggesting it postdates cataclasis (Figure 18). The dark matrix and veinlet may define a corridor of postkinematic fluid flow in the cataclasite. This texture is not apparent in the other sections. However, dark dissolution seams are present in all of the petrographic sections (Figure 17, Figure 18a). The late Eocene age is incompatible with the evidence for ARM movement on the Ouray fault (Pennsylvanian-Permian). It is possible that hydrothermal fluids during the late Eocene could have reset the calcite's U-Pb system, providing this young age.

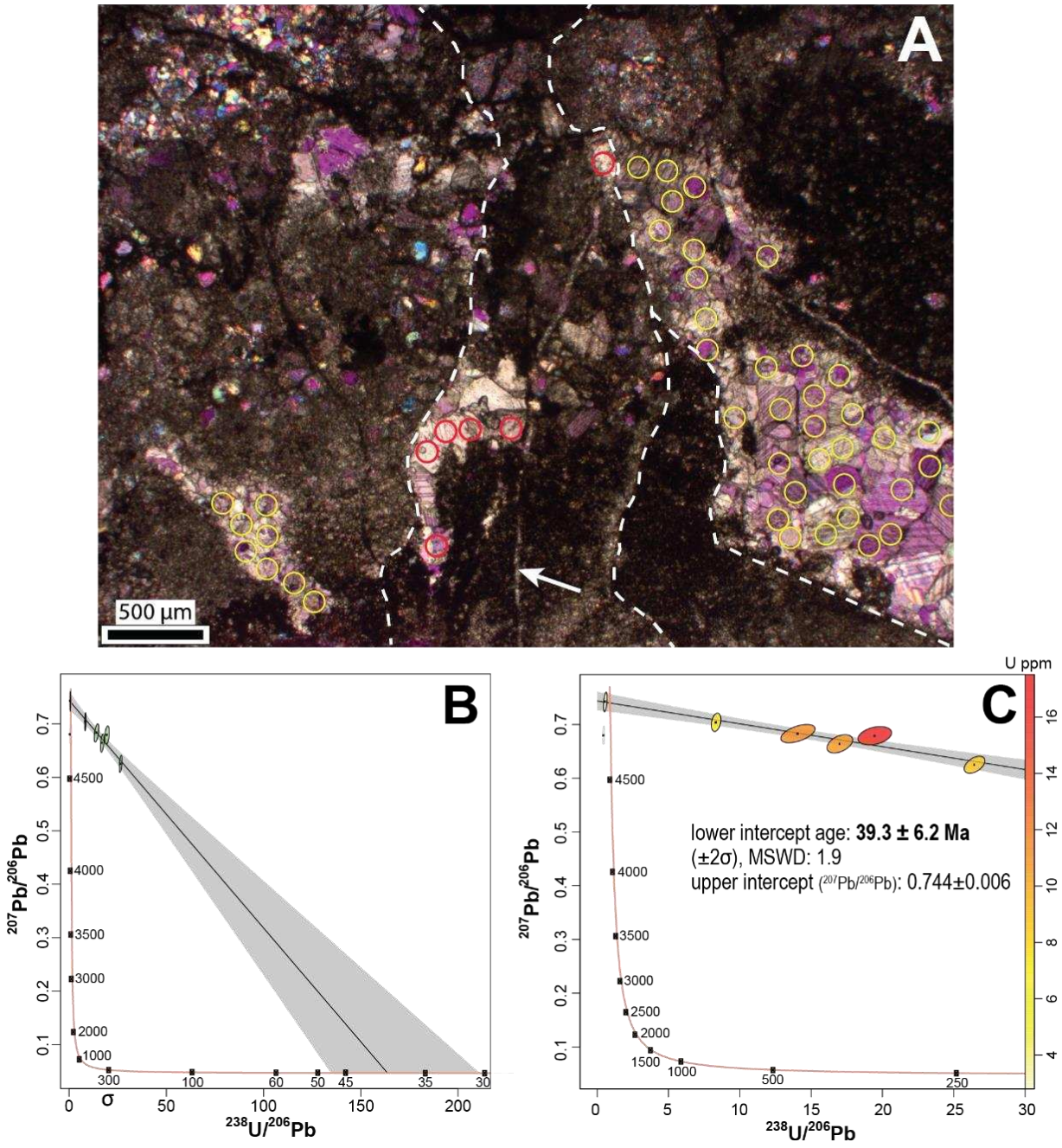

Figure 18. U-Pb geochronology results. A) Photomicrograph of sample E56c showing locations of laser ablation spot locations of U-bearing calcite in red (spot diameters are 110 µm); These 6 spots have 3.3 to 17.0 ppm U, whereas all other analyses (n=44, yellow) have ≤0.07 ppm U. The fluid flow corridor is approximately denoted by the white dashed line. The arrow is pointing to a veinlet which cuts through the fine cataclasite matrix. B) Tera-Wasserburg concordia diagram with linear regression using 6 radiogenic calcite spots and middle Cenozoic lower intercept age. The intercept regression error is ±2σ*√(MSWD); C) Tera-Wasserburg concordia diagram zoomed in on 6 radiogenic calcite spots. The lower intercept age (39.3 ± 6.2 Ma) is interpreted as the calcite age, and the upper intercept is interpreted as the common Pb composition.

3.4 Veins and Joints

Subvertical quartz veins and joints are pervasive across all rock units in the field area (Figure 19). The veins and joints strike NW-SE on average but have a relatively continuous range of strikes from E-W to N-S. The veins have a mean orientation of 157/84°W, and classify as a girdle distribution (G=0.568, P=0.350). The joints have a mean orientation of 161/86°W, and classify as a point distribution (P=0.447, G=0.385). The mean orientation of both the veins and the joints is 159/84°W (Figure 19). This pattern is echoed in the mapped vein trends within units from the Uncompahgre Group through the San Juan Formation with an average trend of ~160° on USGS geologic map GQ-152 (Luedke and Burbank, 1962) (Figure 19k). These extensional features indicate overall NE-SW directed subhorizontal extension in the region.

Adjacent to the Ouray fault in the northern block we commonly observed quartz veins or silicified zones of Leadville Limestone (Figure 20). The veins and joints cut across cataclastic rocks along the Ouray fault and are commonly perpendicular to bedding in the Leadville Limestone. We observed one case where a quartz vein cut across an R-shear on a reverse fault, alluding to the vein postdating the fault.

The veins and joints in Cenozoic volcanic rocks have similar orientations to those in Paleozoic and Mesozoic strata, suggesting that all the extension fractures formed in the Eocene or Oligocene, most likely coevally with magmatism and associated hydrothermal fluid flow. The orientations of veins and joints vary with distance from the Ouray fault. The fractures within 100 m of the Ouray fault are approximately perpendicular to the fault strike, and >100 m from the Ouray fault they primarily strike ~NW-SE to ~E-W (Figure 21).

Some veins contain Cu-Fe mineralization. Many of these are/were targets for prospecting and the occasional adit excavation adjacent to the Ouray fault within the Leadville Limestone (Figure 22). The ore minerals consist of chrysocolla, pyrite and chalcopyrite with gangue minerals typically consisting of quartz, calcite, and barite (Figure 20). This mineralization is common in the region from the Laramide age and subsequent late Eocene to early Miocene magmatism, which emplaced the ample mineral resources throughout the San Juan Mountains.

Within the Uncompahgre Group, the veins are commonly void of Fe-Cu mineralization and consist primarily of quartz (Burbank and Luedke, 2008). In the San Juan Formation, both quartz and calcite veins are present. The calcite veins strike ~NE-SW, whereas the quartz veins and aligned quartz vugs that lack brecciation are oriented approximately subparallel to the Ouray fault. This relationship and the presence of veins that cut the Ouray fault cataclasite zone indicate that both the calcite and quartz veins postdate cataclasis.

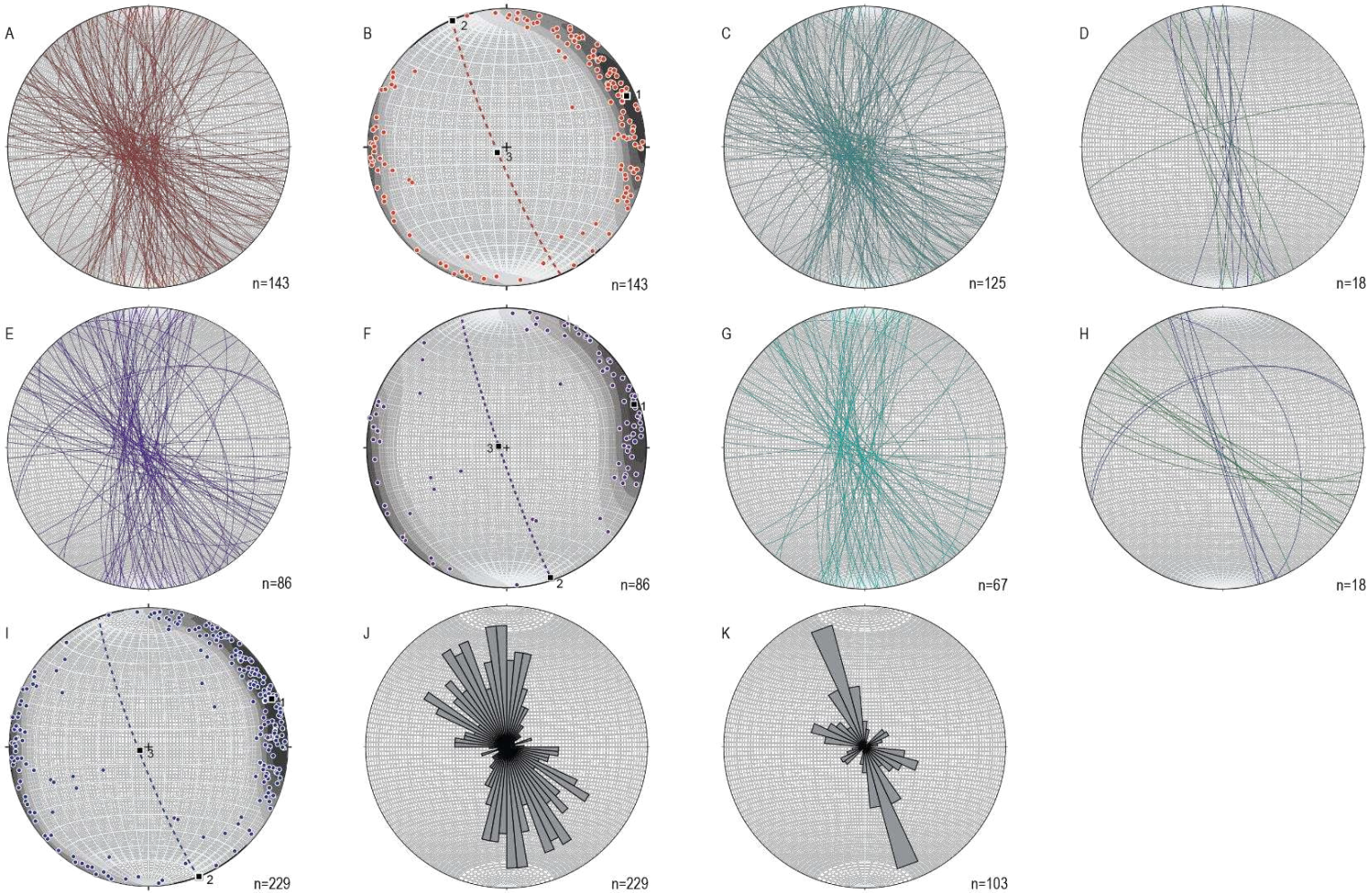

Figure 19. Stereonet plots of quartz veins and joints of the Ouray fault region. Out of the total number of veins (quartz and calcite) measured 86% are in Paleozoic units, 6% are Mesozoic units, and 9% are in Cenozoic units (n=146). Out of the total number of joints measured 5% are in Proterozoic units, 74% are in Paleozoic units, 9% are in Mesozoic units, 12% are in Cenozoic units (n=86). (A) Stereonet plot of all quartz vein planes, which generally strike NW-SE. (B) Poles to quartz veins with the mean plane (157/84°W) and eigenvectors. (C) Quartz veins measured in the Paleozoic units. (D) Quartz veins measured in the Tertiary/Cretaceous granodiorite porphyry (green, n=10), and the Mesozoic sedimentary units (blue, n=8). (E) Joint planes in all units, also generally striking NW-SE. (F) Poles to the joint planes with the mean plane (161/86°W) and eigenvectors. (G) Joint planes in the Paleozoic units. (H) Joints measured in the Tertiary/Cretaceous granodiorite porphyry (green, n=10), and the Mesozoic sedimentary units (blue, n=8). (I) Combined poles to quartz veins and joints in all units with the mean plane (159/84°W) and the eigenvectors (J) Rose diagram of the vein and joint strikes in 5° bins. (J) Rose diagram of mapped vein trends in USGS Quadrangle Map GQ-152 (Luedke and Burbank, 1962) in 10° bins within 1000 m of the mapped area.

Figure 20. Photographs of quartz veins across the region. A) Quartz vein in Leadville Limestone with copper mineralization. B) Quartz vein in Uncompahgre approximately 4 cm thick. C) Quartz vein with euhedral quartz crystals growing in the same direction. D) Veins in the Leadville Limestone.

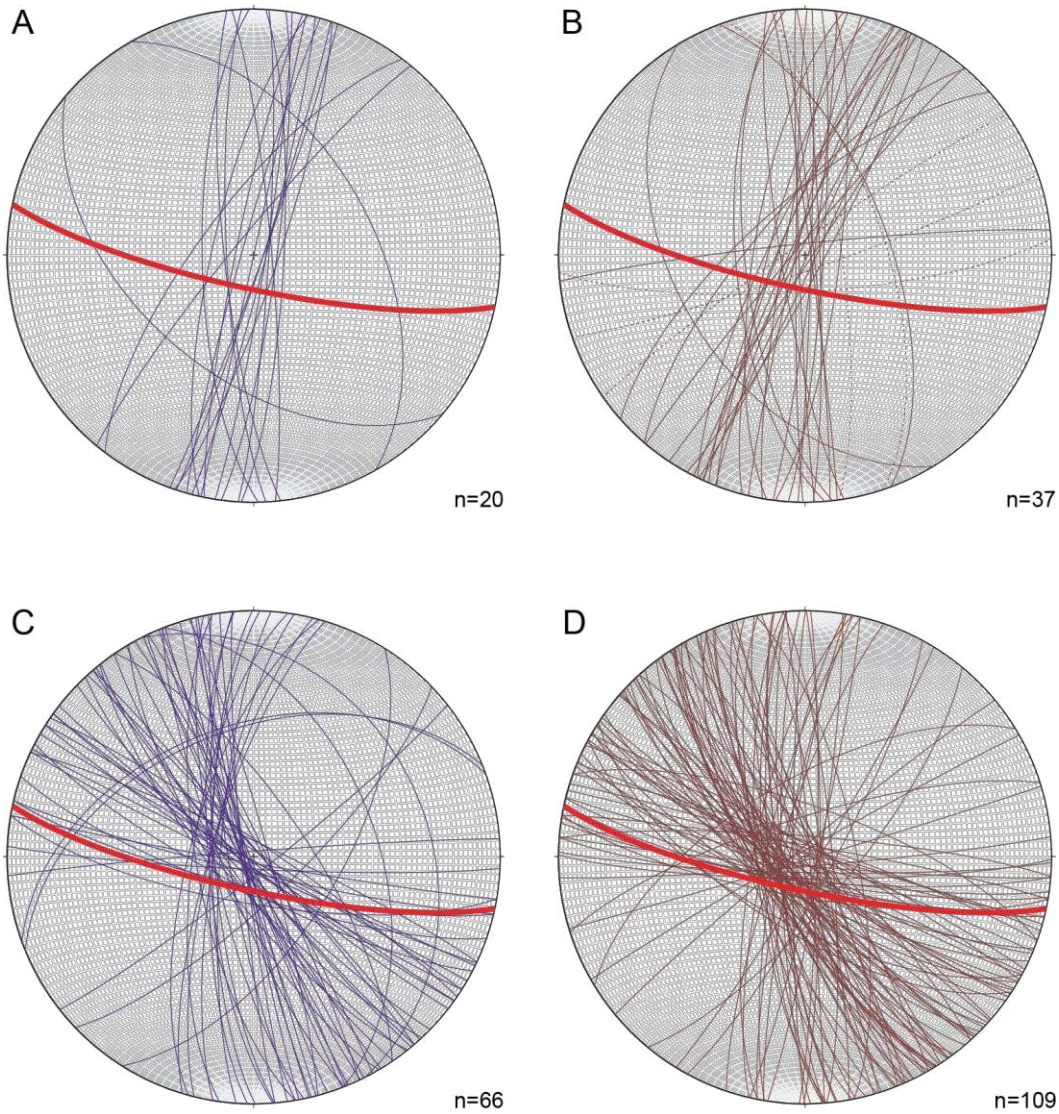

Figure 21. Stereonet plots of extension fractures organized based on distance to the Ouray fault. The mean Ouray fault plane is denoted in red. A) Joints within 100 m of the Ouray fault. B) Veins within 100 m (quartz=solid, calcite=dashed). C) Joints over 100 m from the Ouray fault D) Quartz veins over 100 m.

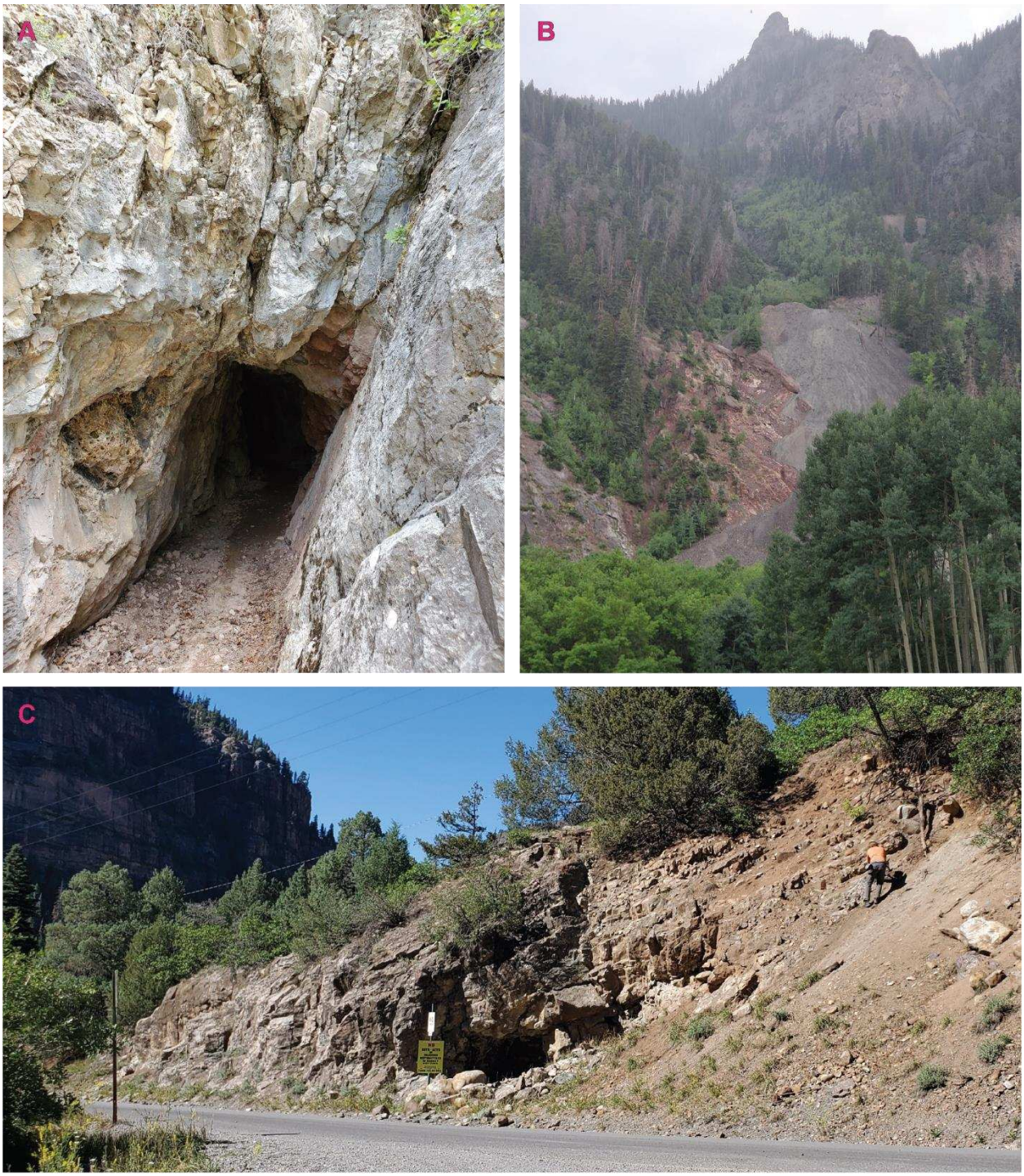

Figure 22. Photographs of mine prospects and claims. A) Mine claim in Leadville Limestone adjacent to the Ouray fault on the western exposure. B) Mine tailings pile with Hermosa Group on the left (north) and Leadville Limestone buried on the right (south) and San Juan Formation above. Ouray fault a little further to the right (south). C) Prospect to the east of Box Canyon in Leadville Limestone; photograph taken on the Ouray fault trace.

4.0 DISCUSSION

4.1 Kinematic Patterns of the Ouray Fault

The WNW-ESE striking, subvertical to steeply-S dipping Ouray fault records obvious S-side-up displacement by juxtaposing the Paleoproterozoic Uncompahgre Group on the south with Mississippian to Pennsylvanian strata to the north. However, the shallowly W-raking slickenlines along the fault record predominantly strike-slip movement. For the Ouray fault to achieve approximately 150–200 m of S-side up movement with the preserved slip indicators, the fault displacement is ~600–800 m of oblique sinistral/S-side-up slip. Adjacent small-scale faults dominantly strike E-W to NW-SW and record sinistral, reverse, or oblique-sinistral slip. The P-axis distribution is consistent with NE-SW shortening, and the girdle distribution of T-axes record extension along NW-SE striking plane (Figure 12). The fault plane solution records sinistral-reverse slip on a WNW-striking fault. All of these data support sinistral transpression kinematics in the Ouray fault region.

The syncline within the Leadville Limestone is an additional indicator of sinistral transpression (Figure 9). Researchers have established that folds formed under strike-slip conditions initiate at ~45° from the primary fault, where in transpression the folds form at an angle <45° and as deformation continues the fold axes will rotate towards the fault (e.g., Odonne and Vialon, 1983; Jamison, 1991; Tikoff and Peterson, 1998; Ghosh et al., 2014). In the case of sinistral movement, the fold rotates counterclockwise towards the fault. The sinuous pattern of this syncline mimics this pattern with a tight subparallel fold closest to the fault, then opening up and oriented ~45° from the fault (Figure 9). The ~45° angle between the fault and the syncline trace was likely the original orientation of the fold formed under predominantly strike-slip movement. As deformation continued the fold rotated counterclockwise towards the fault (Figure 23), followed by the Ouray fault breaking through the Paleozoic strata. The subparallel section of the syncline adjacent to the fault could have been amplified as a fault-propagation fold as the Ouray fault broke through the Leadville Limestone strata. The monocline in Devonian strata along the south side of Ouray fault at Box Canyon likely represents a fault-propagation fold as the Ouray fault propagated from the Uncompahgre Group into the Paleozoic strata (Figure 23). However, the monocline

axis also appears to trend clockwise of the Ouray fault, suggesting this fold may have also initiated during sinistral shear.

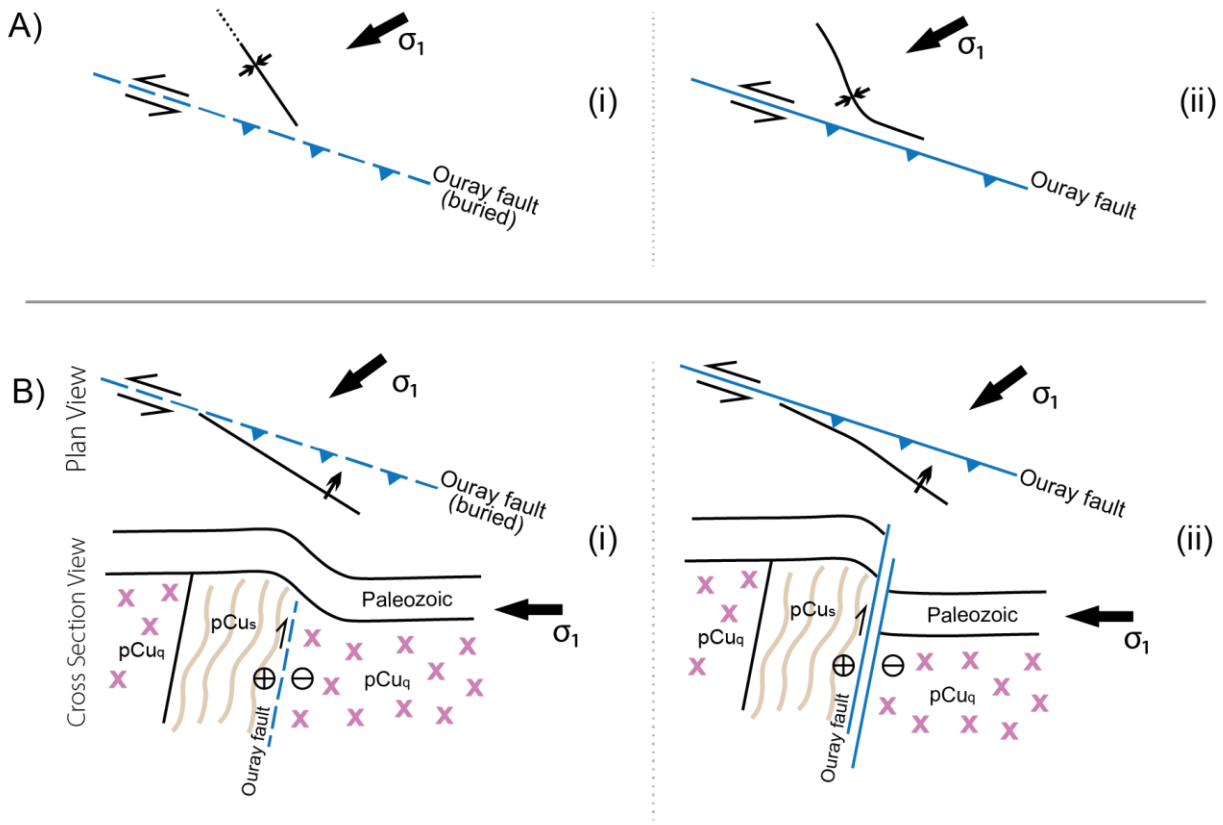

Figure 23. Potential models for fold formation. A) Sinistral transpression initiating the fold <45° from the buried fault (i), followed by the fold rotating counterclockwise subparallel to the fault (ii). B) Monocline forming adjacent to the buried fault (i), followed by the fault breaking through strata, resulting in cessation of folding on the monocline (ii). Cross sections show the + in a circle as moving towards the viewer, the – in a circle is moving away. Triangles on the fault indicate the direction of the up-thrown block.

The distal (>100 m) small-scale faults around the Ouray fault record more variable kinematics, but still record a dominant NE-SW shortening direction and a fault plane solution indicative of oblique sinistral-reverse slip on E-W to NW-SE striking planes (Figure 16). All of the recorded reverse and sinistral faults record approximately the same shortening directions (Figure 13, Figure 14). Oblique sinistral-reverse faults are also common, suggesting the sinistral and reverse-slip regimes were coeval. Combined, the sinistral, reverse, and oblique-slip faults record 3-dimensional strain with NE-SW shortening, and multiple extension orientations ranging from subvertical to subhorizontal NW-SE

extension, or more generally a subvertical extensional “plane” striking NW-SE. This strain pattern can also be described in the form of an oblate 3D strain ellipsoid with a short axis trending NE-SW.

4.2 Structural Evolution of the Ouray Fault

The steep overall dip of faults in the Uncompahgre Group and the abundance of bedding-parallel faults suggests that the Ouray fault and surrounding minor faults were strongly influenced by preexisting steep bedding from Proterozoic folding. Bedding-parallel faults propagated into the Paleozoic units, consistently cutting across the more gently-dipping bedding.

This inherited structural grain in the Uncompahgre Group most likely influenced fault kinematics in addition to fault plane geometry. To accommodate NE-SW shortening across this area, it was apparently easier to do so through sinistral slip along the existing subvertical E-W to ESE-WNW-striking bedding and lithologic layering in Uncompahgre Group rather than forming new NW-SE striking reverse faults. It is likely that a homogeneous basement or one with a different structural grain would have recorded a different geometry and kinematics during brittle ARM faulting.

Marshak et al. (2000) propose that rifting features formed during the Mesoproterozoic and Neoproterozoic created permanent weaknesses in the crust. Subsequent orogenies (ARM and Laramide) likely reactivated these extensional structures with regional reverse, oblique, and strike-slip movements. Prior to the rifting events, Karlstrom et al. (2017) indicate that there were at least three folding/shortening events which likely created the subvertical bedding orientations we observe in the Uncompahgre Group. The emplacement of the diabase dike in the Ouray fault region likely occurred during NE-SW or NNW-SSE Proterozoic extension.

In the Grenadier block to the south, Thomas (2007) determined that the Ignacio Quartzite is missing from the up-thrown block between the Coal Bank Pass fault and the Molas Creek fault zone. This observation suggests that these ARM faults may have reactivated Late Devonian (pre-Elbert Formation) faults that may have been precursors to the ARM. Thomas (2007) also noted that there is a strong relationship between the orientation of the Uncompahgre Group layers and overlying Paleozoic fold and fault orientations, that the Hermosa Group was syndepositional with the Snowdon fault, and that the ARM faults in the Grenadier block record sinistral slip and transpression during the ARM deformation.

There are many similarities between the Ouray fault and the faults of the Grenadier block. The Ouray fault records NE-SW shortening via sinistral transpression, and it likely inherited its geometry from the Uncompahgre Group's orientation and lithologic weaknesses, such as the weaker phyllite interval which it follows for most of its exposure (Plate 2). We were not able to determine if the Hermosa Group was syndepositional with the Ouray fault movement due to its poor exposure near the fault.

Slip on the Ouray fault ceased prior to the Mesozoic based on the onlapping of relatively undeformed Triassic strata, and potentially the Permian (Plate 2). The Permian Cutler Formation is largely buried by glacial and other Quaternary sedimentary deposits, making for poor exposures along the projected Ouray fault trace. Because of the poor exposure and lack of field evidence, I mapped the Ouray fault as ending in the Pennsylvanian strata (Plate 2). This interpretation supports the Sweet et al. (2021) ARM basin analysis indicating that most ARM deformation occurred in the Pennsylvanian. However, the angular unconformity between the Permian Cutler Formation and the Triassic Dolores Formation (Figure 3a) indicates a period of folding/tilting into the Permian and ending prior to the Mesozoic era. Alternatively, the lack of evidence of the Ouray fault extending into the Cutler Formation may be because the offset of the fault dies out westward in the Cutler Formation with no surface expression. On the Snowdon and Coal Bank Pass faults, Thomas (2007) also did not observe the continuation of these faults into the Cutler Formation. Additional detailed mapping and kinematic data are needed to evaluate whether deformation occurred primarily in the Pennsylvanian or continued into the Permian.

During regional magmatism in the Laramide (Late Cretaceous and Paleocene/Early Eocene) and in late Eocene to early Miocene, the Ouray fault appears to have been a conduit for fluid flow. The calcite U-Pb age of 39.3 ± 6.2 Ma from vein fragments on the Ouray fault plane indicates late Eocene fluid flow. The relationship of the high U LA-ICP-MS analysis spots, located within a dark corridor, and a majority of the spots in one vein fragment (central) with one spot in another vein fragment (right), indicates that fluid flow in the corridor likely reset the U-Pb system (Figure 18a). In conjunction, the relatively low MSWD value for these U-Pb analyses indicates only one population of calcite of this age (Figure 18). The evidence for post-kinematic fluid flow is also supported by the presence of a post-cataclasis calcite veinlet in the high U zone (Figure 18a), and more generally by the abundance of veins and joints oriented subvertically N-S to subparallel to the Ouray fault, as they are found in all of the units within the region

and appear to postdate cataclasis on the Ouray fault (Figure 19, Figure 20). During primarily NE-SW Cenozoic extension the stress field likely rotated adjacent to the Ouray fault, orienting σ_3 and the extension axis parallel to the weak Ouray fault (WNW-ESE) and forming subvertical veins and joints approximately perpendicular to the fault (Figure 20, Figure 21). The NW-SE striking normal faults match the kinematic patterns of the veins and joints at distance from the Ouray fault, indicating that the normal faulting may have occurred coevally with these extensional fractures. The NE-SW to E-W extension associated with the normal faults, veins and joints may have occurred during Eocene-Oligocene magmatism and/or potentially the early stages of the Rio Grande rift in the late Oligocene to early Miocene.

4.3 Kinematic Impacts on the ARM System

The Ouray fault can be considered a preserved ARM fault (e.g., not overprinted by the Laramide orogeny). There is no evidence that the Ouray fault was active following the Permian. The kinematics collected on the Ouray fault and the small-scale faults in the vicinity support recent tectonic models of sinistral transpression along the southwestern margin of the ARM system with NE-SW shortening (Leary et al., 2017; Sweet et al., 2021). The Leary et al. (2017) ARM kinematic model (Figure 1b) provides a very similar pattern to the kinematics observed around the Ouray fault (Figure 24).

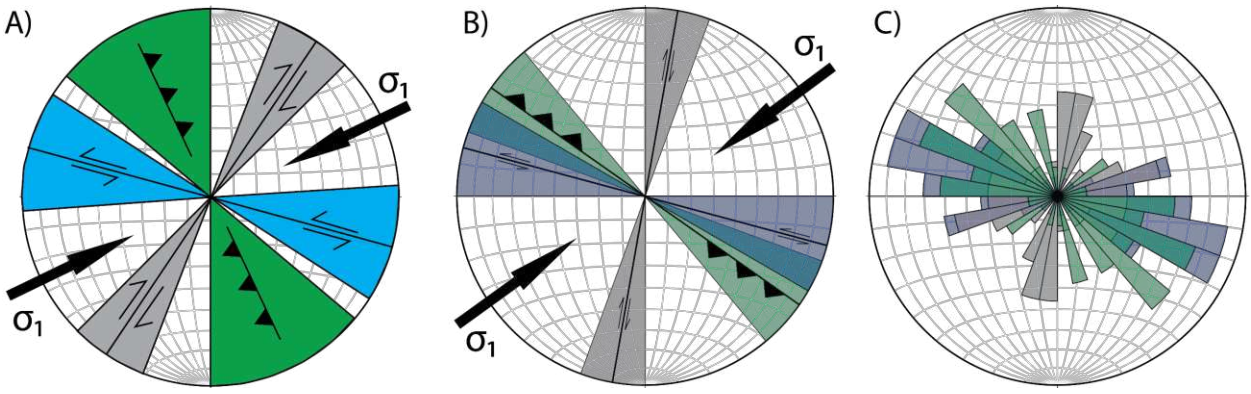

Figure 24. A) Kinematic model from Leary et al. (2017) from data collected in the Central Basin Platform (Shumaker, 1992) to predict orientations of ARM faults that may have formed in response to a regional NE-SW directed maximum stress (also see Figure 1). B) Kinematic model of the Ouray fault data based on the strikes of the strike-slip and reverse faults. C) Rose diagram of the fault strikes for sinistral, dextral and reverse faults. Blue = sinistral (n=49), green = reverse (n=32), and gray = dextral (n=27).

The ARM system consists of variable geometries and kinematics over its 1,500-kilometer extent. It is highly likely that this basement-cored orogeny has been readily influenced by preexisting structures in the basement rocks. Marshak et al. (2000) discusses at least three pre-ARM episodes of extension with the resulting normal faults striking NW-SE to N-S in the basement core.

Kinematic data presented here are consistent with the work by Thomas (2007) in the Grenadier fault block ~30 km south of the Ouray fault, where folds and E-W to SE-NW high-angle faults are interpreted to record sinistral transpression. The geometry of these faults preserves a relationship with the basement orientations. The Picuris-Pecos fault in New Mexico may be another example of potential preexisting structural control on ARM faults (Figure 2). Cather et al. (2011) have confirmed that the Picuris-Pecos fault could have initiated during the Grenville orogeny (~1.2–0.9 Ga) or younger rifting events. The Picuris-Pecos fault was active during the middle Pennsylvanian as an ARM-bounding fault on the Taos trough in northern New Mexico, recording ~37 km of dextral slip (Cather et al., 2011). The Picuris-Pecos fault trend and slip sense are consistent with the modeled kinematics in Figure 24.

Most observable ARM structures appear to be consistent with a NE-SW maximum stress direction. The heterogenous basement rocks and pre-ARM deformation likely gave rise to kinematic complexity during ARM deformation; however, sinistral, dextral, and reverse sense faults may all record NE-SW shortening proposed for the ARM system. Future ARM tectonic models should account for the widespread evidence of NE-SW shortening.

5.0 CONCLUSIONS

The WNW-ENE Ouray fault preserves ARM deformation geometry and kinematics that have been strongly influenced by the preexisting steeply-dipping structural grain in the Paleoproterozoic Uncompahgre Group. The Ouray fault ranges from steeply dipping to the south at its eastern extent to subvertical at its western exposure. The principal slip plane records oblique sinistral-reverse slip with approximately 600–800 m of displacement. Kinematically, the Ouray fault and surrounding small-scale faults record a history of NE-SW shortening with an extensional plane oriented subvertically NW-SE, consistent with sinistral transpression along the Ouray fault. Based on similarity with other likely ARM structures in the region, sinistral transpression may have been the dominant ARM kinematic regime along the southwestern margin of the Uncompahgre uplift.

Post-kinematic fluids appear to have used the Ouray fault as a conduit during the late Eocene based on a calcite U-Pb geochronology date. Additionally, the extension fractures appear to be post-kinematic as well, where they are commonly perpendicular to the Ouray fault, cut across cataclasite, and are widespread throughout all geologic units including Oligocene volcanics.

6.0 FUTURE RESEARCH

The lack of kinematic data on ARM structures is primarily a result of Laramide overprinting; however, preserved ARM structures are present and should be studied in greater detail. Potential projects to continue ARM research on the Ouray fault region and the greater ARM system include:

1. Perform calcite U-Pb geochronology dating at additional locations along the Ouray fault and small-scale faults with similar kinematics to better constrain the timing of faulting in the region. The surrounding smaller scale faults may be less susceptible to fluid flow resetting. Collecting U-Pb dates on calcite veins in the region may also help to constrain their timing in relation to faulting.
2. Add to and update the detailed geologic map of the region, improving constraints on the locations of the Uncompahgre phyllite, map-scale folds and the faults within the Uncompahgre Group, and potential exposures of the Ouray fault in the Cutler Formation and overlying units west of Box Canyon.
3. Perform a sedimentological/stratigraphical study of the Hermosa Group and Cutler Formation adjacent to the Ouray fault to evaluate how sedimentation patterns may have been affected by Pennsylvanian-Permian slip on the Ouray fault. This work would be a challenging due to the locally steep topography and heavy vegetation and colluvial deposits above and around the Ouray fault. The field area would likely need to be expanded to include areas where the Hermosa Group is better exposed (e.g., the canyon exposures to the north of the Ouray fault, west of Ouray).
4. Perform a kinematic study of other potential ARM faults in the Grenadier block to both confirm the Thomas (2007) findings and to add to the kinematic data set of ARM structures.
5. The Ouray fault and the faults of the Grenadier block have a relatively anomalous E-W orientation compared to the rest of the Uncompahgre uplift. This ~E-W orientation follows the basement rocks structural grain. Observing other areas along strike of the SW margin of the Uncompahgre uplift and structural blocks to the south with differing structural grain could test the idea that inherited structures influenced the kinematics in the region.

7.0 REFERENCES

Allmendinger, R. W., Cardozo, N., and Fisher, D., 2012, *Structural geology algorithms: Vectors and tensors in structural geology*. Cambridge University Press.

Allmendinger, R.W, Siron, C.R. and Scott, C.P., 2017, Structural data collection with mobile devices: Accuracy, redundancy, and best practices. *Journal of Structural Geology,* v. 102, p. 89–112.

Baars, D.L., and See, P.D., 1968, Pre-Pennsylvanian stratigraphy and paleotectonics of the San Juan Mountains, southwestern Colorado. *Geological Society of America Bulletin*, v. 79, p. 333–349.

Barbeau, D.L., 2003, A flexural model for the Paradox Basin: Implications for the tectonics of the Ancestral Rocky Mountains. *Basin Research*, v. 15, p. 97–115

Budnik, R.T., 1986, Left-lateral intraplate deformation along the ancestral Rocky Mountains: Implications for late Paleozoic plate motions. *Tectonophysics*, v. 132, p. 195–214.

Burbank, W.S. and Luedke, R.G., 2008, Geology and Ore Deposits of the Uncompahgre (Ouray) Mining District, Southwestern Colorado. US Geological Survey, Professional Paper 1753.

Caine, J.S., Nelson, E.P., Beach, S.T., and Layer, P.W., 2006, Structural fabrics, mineralization, and Laramide kinematics of the Idaho Springs-Ralston shear zone, Colorado mineral belt and central Front Range uplift. *The Mountain Geologist*, v. 43, p. 1–24.

Cardozo, N., and Allmendinger, R.W., 2013, Spherical projections with OSXStereonet. *Computers & Geosciences*, v. 51, p. 193–205.

Cather, S.M., Read, A.S., Dunbar, N.W., Kues, B.S., Krainer, K., Lucas, S.G., and Kelley, S.A., 2011, Provenance evidence for major post–early Pennsylvanian dextral slip on the Picuris-Pecos fault, northern New Mexico. *Geosphere*, v. 7 (5), p. 1175–1193.

De Voto, R. H., B. L. Bartleson, C. J. Schenk, and N. B. Waechter, 1986, Late Paleozoic stratigraphy and syndepositional tectonism, northwestern Colorado. In: *New interpretations of northwest Colorado geology*: Stone, D.S. ed., Rocky Mountain Association of Geologists Symposium Volume, p. 37–49.

Dickinson, W.R., and Lawton, T.F., 2003, Sequential intercontinental suturing as the ultimate control for Pennsylvanian Ancestral Rocky Mountains deformation. *Geology*, v. 31, p. 609–612.

Erslev, E. A., 2001, Multistage, multidirectional Tertiary shortening and compression in north-central New Mexico. *Geological Society of America Bulletin*, v. 113, p. 63–74.

Erslev, E.A., and Koenig, N.V., 2009, Three-dimensional kinematics of Laramide, basement-involved Rocky Mountain deformation, U.S.A.: Insights from minor faults and GIS-enhanced structure maps: Boulder, Colorado. *Geological Society of America Memoir*, v. 204, p. 125–150.

Ewing, T.E., 2017, Laramide and Cenozoic structural and paleotopographic history of the Ouray area and the northwestern flank of the San Juan Mountains, Colorado. In: *The Geology of the Ouray-Silverton Area*: Karlstrom, K.E.; Gonzales, D.A.; Zimmerer, M.J.; Heizler, M.; Ulmer-Scholle, D.S. eds., New Mexico Geological Society 68th Annual Fall Field Conference Guidebook, p. 169–178.

Frahme, C.W., and Vaughn, E.B., 1983, Paleozoic geology and seismic stratigraphy of the northern Uncompahgre Front, Grant County, Utah. Field Conference – Rocky Mountain Association of Geologists, v. 1983, p. 201–211.

Ghosh, N., Chakra, M., and Chattopadhyay, A., 2014, An experimental approach to strain pattern and folding in unconfined and/or partitioned transpressional deformation. *International Journal of Earth Sciences*, v. 103, p. 349–365.

Hoy, R.G., and Ridgway, K.D., 2002, Syndepositional thrust-related deformation and sedimentation in an Ancestral Rocky Mountains basin, central Colorado trough, USA. *Geological Society of America Bulletin*, v. 114, p. 804–828.

Jamison, W.R., 1991, Kinematics of compressional fold development in convergent wrench terranes. *Tectonophysics*, v. 190, p. 209–232.

Karlstrom, K.E., Gonzales, D.A., Heizler, M., and A. Zinnser, 2017, $^{40}Ar/^{39}Ar$ age constraints on the deposition and metamorphism of the Uncompahgre Group, southwestern Colorado. In: *The Geology of the Ouray-Silverton Area*, Karlstrom, K.E.; Gonzales, D.A.; Zimmerer, Matthew J.; Heizler, M.; Ulmer-Scholle, D.S. eds., New Mexico Geological Society 68th Annual Fall Field Conference Guidebook, p. 83–90.

Kuth, C.F., 1986, Plate tectonics of the Ancestral Rocky Mountains. In: *Paleotectonics and sedimentation in the Rocky Mountain region, United States*: Peterson, J.A. ed., AAPG Memoir.

Kluth, C.F., 1997, Comparison of the location and structure of the Late Paleozoic and Late Cretaceous-Early Tertiary Front Range uplift. *Colorado Front Range Guidebook*, Rocky Mountain Association of Geologists, p. 31-–42.

Kluth, C.F., 1998, Late Paleozoic deformation of interior North America: The greater Ancestral Rocky Mountain. *American Association of Petroleum Geologists Bulletin*, v. 82, p. 2272–2276.

Kluth, C.F., and Coney, P.J., 1981, Plate tectonics of the ancestral Rocky Mountains. *Geology*, v. 9, p. 10–15.

Kylander-Clark, A.R., 2020, Expanding the limits of laser-ablation U–Pb calcite geochronology. *Geochronology*, v. 2 (2), p.343–354.

Larsen, E.S. Jr., and Cross, W., 1956, Geology and Petrology of the San Juan Region, Southwestern Colorado. U.S. Geological Survey Professional Paper 258.

Lawton, T.F., Cashman, P.H., Trexler, J.H., and Taylor, W.J., 2017, The late Paleozoic Southwestern Laurentian Borderland. *Geology*, v. 45 (8), p. 675–678.

Lawton, T., Thomas, W.A., and Blakey, R.C., 2020, Tapping Texas into place; a parautochthonous indenter mechanism for the ancestral Rocky Mountains orogen. *Abstracts with Programs - Geological Society of America,* v. 52 (6): Abstract no. 198-12.

Leary, R.J., Umhoefer, P., Smith, M.E., and Riggs, N., 2017, A three-sided orogen: A new tectonic model for Ancestral Rocky Mountain uplift and basin development. *Geology*, v. 45, p. 735–738.

Leary, R.J., Umhoefer, P., Smith, M.E., Smith, T.M., Saylor, J.E., Riggs, N., Burr, G., Lodes, E., Foley, D., Licht, A., Mueller, M.A., and Baird, C., 2020, Provenance of Pennsylvanian–Permian sedimentary rocks associated with the Ancestral Rocky Mountains orogeny in southwestern Laurentia: Implications for continental-scale Laurentian sediment transport systems. *Lithosphere*, v. 12 (1), p. 88–121.

Luedke, R.G., and Burbank, W.S., 1962, Geology of the Ouray quadrangle, Colorado. U.S. Geological Survey, Geologic Quadrangle Map GQ-152, scale 1:24,000.

Luedke, R.G., and Burbank, W.S., 1981, Geologic Map of the Uncompahgre (Ouray) Mining District, southwestern Colorado. U.S. Geological Survey Miscellaneous Investigations Series Map I-1247.

Marrett, R., and Allmendinger, R.W., 1990, Kinematic analysis of fault-slip data. *Journal of Structural Geology*, v. 12, p. 973–986.

Marshak, S., Karlstrom, K., and Timmons, J.M., 2000, Inversion of Proterozoic extensional faults: An explanation for the pattern of Laramide and Ancestral Rockies intracratonic deformation, United States. *Geology*, v. 28 (8), p. 735–738.

McBride, E.F., 2016, Stratigraphy, petrography, and depositional history of the Ignacio Quartzite and McCracken Sandstone Member of the Elbert Formation, southwestern Colorado, U.S.A. *Rocky Mountain Geology*, v. 51 (2), p. 23–68.

McConnell, D.A., 1989, Determination of offset across the northern margin of the Wichita uplift, southwest Oklahoma. *Geological Society of America Bulletin*, v. 101, p. 1317–1332.

Miranda, T.S., Neves, S.P., Celestino, M.A.L., and Roberts, N.M.W., 2020, Structural evolution of the Cruzeiro do Nordeste shear zone (NE Brazil): Brasiliano-Pan-African- ductile-to-brittle transition and Cretaceous brittle reactivation. *Journal of Structural Geology*, v. 141, 104203

Moore, K.D., Soreghan, G.S., and Sweet, D.E., 2008, Stratigraphic and structural relations in the proximal Cutler Formation of the Paradox basin: Implications for the timing of movement on the Uncompahgre front. *Mountain Geologist*, v. 45, p. 49–68.

Nuriel, P., Weinberger, R., Kylander-Clark, A.R.C., Hacker, B.R., and Craddock, J.P., 2017, The onset of the Dead Sea transform based on calcite age-strain analyses. *Geology*, v. 45 (7): p. 587–590.

Nuriel, P., Craddock, J., Kylander-Clark, A.R.C., Uysal, I.T., Karabacak, V., Dirik, R.K., Hacker, B.R., and Weinberger, R., 2019, Reactivation history of the North Anatolian fault zone based on calcite age-strain analyses. *Geology*, v. 47 (5), p. 465–469.

Nuriel, P., Wotzlaw, J.F., Ovtcharova, M., Vaks, A., Stremtan, C., Šala, M., Roberts, N.M. and Kylander-Clark, A.R., 2021, The use of ASH-15 flowstone as a matrix-matched reference material for laser-ablation U−Pb geochronology of calcite. *Geochronology*, v. 3 (1), p.35–47.

Odonne, F. and Vialon, P., 1983, Analogue models of folds above a wrench fault. *Tectonophysics*, v. 99, p. 31–46.

Petit, J. P., 1987, Criteria for the sense of movement on fault surfaces in brittle rocks. *Journal of Structural Geology*, v. 9, p. 597–608.

Ring, U., and Gerdes, A., 2016, Kinematics of the Alpenrhein-Bodensee graben system in the Central Alps: Oligocene/Miocene transtension due to formation of the Western Alps arc. *Tectonics*, v. 35, p. 1367–1391.

Roberts, N. M. W., Drost, K., Horstwood, M. S. A., Condon, D. J., Chew, D., Drake, H., Milodowski, A. E., McLean, N. M., Smye, A. J., Walker, R. J., Haslam, R., Hodson, K., Imber, J., Beaudoin, N., and Lee, J. K., 2020, Laser ablation inductively coupled plasma mass spectrometry (LA-ICP-MS) U–Pb carbonate geochronology: strategies, progress, and limitations. *Geochronology*, v. 2, p. 33–61.

Roberts, N.M.W., and Walker, R.J., 2016, U-Pb geochronology of calcite-mineralized faults: Absolute timing of rift-related fault events on the northeast Atlantic margin. *Geology*, v. 44 (7), p. 531–534.

Roberts, N.M.W., Žák, J., Vacek, F., and Sláma, J., 2021, No more blind dates with calcite: Fluid-flow vs. fault-slip along the Očkov thrust, Prague Basin. *Geoscience Frontiers*, v. 12 (4), 101143.

Shumaker, R.C., 1992, Paleozoic structure of the Central Basin uplift and adjacent Delaware basin, west Texas. *American Association of Petroleum Geologists Bulletin*, v. 76, p. 1804–1824.

Singleton, J.S., Mavor, S.P., Seymour, N.M., Williams, S.A., Patton, A.I., Ruthven, R.C., Johnson, E.P., and Prior, M.G., 2019, Laramide shortening and the influence of Precambrian basement on uplift of the Black Hills, South Dakota and Wyoming, U.S.A. *Rocky Mountain Geology*, v. 54 (1), p. 1–17.

Sitar, M. C. 2020, Unpublished Python script for bulk eigenvector-averaging of structural data using mplstereonet. From Kington, J., 2020, mplstereonet package https://github.com/joferkington/mplstereonet (accessed September 2020).

Soreghan, G.S., Keller, G.R., Gilbert, M.C., Chase, C.G., and Sweet, D.E., 2012, Load induced subsidence of the Ancestral Rocky Mountains recorded by preservation of Permian landscapes. *Geosphere*, v. 8, no. 3, p. 654–668.

Steven, T.A., and Lipman, P.W., 1976, Calderas of the San Juan Volcanic Field, Southwestern Colorado. U.S. Geological Survey Professional Paper 958.

Stevenson, G.M., and Baars, D.L., 1986, The Paradox: A pull-apart basin of Pennsylvanian age. In: *Paleotectonics and Sedimentation*: Peterson, J.A., ed., *American Association of Petroleum Geologists Memoir*, v. 41, p. 513–539.

Stone, D.S., 1977, Tectonic history of the Uncompahgre Uplift. In: *Exploration frontiers of the central and southern Rockies*: Veal, H.K., ed. Field Conference – Rocky Mountain Association of Geologists, v. 1977, p. 23–30.

Sweet, D.E., Brotherton, J.L., Chowdhury, N.U.M.K., and Ramsey, C.E., 2021, Tectonic subsidence analysis of the Ancestral Rocky Mountains from the interior to the southern margin. *Palaeogeography, Palaeoclimatology, Palaeoecology*, v. 576 (15), p. 1–16.

Sweet, D.E., Carsrud, C.R., and Watters, A.J., 2015, Proposing an entirely Pennsylvanian age for the Fountain Formation through new lithostratigraphic correlation along the Front Range. *Mountain Geologist,* v. 52, p. 43–70.

Sweet, D.E., and Soreghan, G.S., 2010, Late Paleozoic tectonics and paleogeography of the ancestral Front Range: Structural, stratigraphy and sedimentologic evidence from the Fountain Formation (Manitou Springs, Colorado). *Geological Society of America Bulletin*, v. 122, p. 575–594.

Thomas, W.A., 2007, Pennsylvanian sinistral faults along the southwest boundary of the Uncompahgre uplift, Ancestral Rocky Mountains, Colorado. *Geosphere*, v. 3, p. 119–132.

Tikoff, B., and Peterson, K., 1998, Physical experiments of transpressional folding. *Journal of Structural Geology*, v. 20 (6), p. 661–672.

Turko, M. and Mitra, S., 2021, Macroscopic Structural Styles in the Southeastern Anadarko Basin, Southern Oklahoma. *Marine and Petroleum Geology*, v. 125, 104863.

Tweto, O.L., and Lovering, T.S., 1977, Geology of the Minturn 15-minute quadrangle, Eagle and Summit counties, Colorado. US Geological Survey Professional Paper, PP-956.

Vollmer, F.W., 1990, An application of eigenvalue methods to structural domain analysis. *GSA Bulletin*, v. 102 (6), p. 786–791.

Wachter, N. B., and W. E. Johnson, 1986, Pennsylvanian–Permian paleostructure and stratigraphy as interpreted from seismic data in the Piceance basin, northwest Colorado. In: *New interpretations of northwest Colorado geology*: Stone, D.S. ed., Rocky Mountain Association of Geologists Symposium Volume, p. 51–64.

Weil, A.B., and Yonkee, A., 2012, Layer-parallel shortening across the Sevier fold-thrust belt and Laramide foreland of Wyoming: spatial and temporal evolution of a complex geodynamic system. *Earth and Planetary Science Letters,* 357-358, p. 405-420.

Weimer, R.J., 1980, Recurrent movement on basement faults, a tectonic style for Colorado and adjacent areas. In: *Colorado Geology*: Kent, H.C., and Porter, K.W., eds., Rocky Mountain Association of Geologists, p. 23–35.

Ye, H.Z., Royden, L., Burchfiel, C., and Schuepbach, M., 1996, Late Paleozoic deformation of interior North America: The greater Ancestral Rocky Mountains. *American Association of Petroleum Geologists Bulletin*, v. 80, p. 1397–1432.